Magmatic systems, fluid magmatic interaction, melts properties

[#]Litvin Yu.A., Aldushin K.A. Diamond synthesis in carbonate melts of the $(Li,Na,K)_2(Ca,Mg)(CO_3)_2$ - graphite system at 8.5 - 9.5 GPa.

key words [*diamond carbonates synthesis experiment pressure*]

The $(Li,Na,K)_2(Ca,Mg)(CO_3)_2$ system is of interest for a high pressure synthesis of diamonds as it is compositionally close to fluid inclusions in natural diamonds [1] being solutions wherefrom diamonds crystallized in the Earth's mantle. The concentrations of the basic components in these solutions vary: SiO_2 23.9 - 52.3, TiO_2 4.2 - 5.1, Al_2O_3 2.0-6.2, FeO 8.8-17.5, MgO 4.4-10.9, CaO 3.2-16.3, Na_2O 0.3-3.0, K_2O 11.5 - 22.2, P_2O_5 0.5-2.6 Cl 0.7-1.7 (wt%), and the fluid contents are within the ranges: H_2O 19-506 (ppm) and CO_2 15-940 (ppm). The compositions of the inclusions are approximated [1] by two model boundary compositions - water - siliceous (SiO_2 58.4, TiO_2 4.3, Al_2O_3 6.8, FeO 7.6, MgO 3.3, CaO 0.0, Na_2O 2.2, K_2O 12.3, P_2O_5 0.7, Cl 0.9) and carbonatite (SiO_2 13.6, TiO_2 4.6, Al_2O_3 0.8, FeO 19.5, MgO 13.2, CaO 20.5, Na_2O 2.2, K_2O 20.7, P_2O_5) 2.4, Cl 1.3 wt%). In molecular expression the basic components of the carbonatite composition are K_2O, Na_2O, CaO, MgO, FeO, CO_2. This is suggestive of search for new processes of diamond synthesis in alkali carbonate systems, primarily, in the $K_2Ca(CO_3)_2$-$Na_2Ca(CO_3)_2$-C system. Synthesis of diamond in the lithium system $Li_2Ca(CO_3)_2$ - $Li_2Mg(CO_3)_2$ -C is of importance for the problem concerned with diamond crystal growth in carbonate-carbon systems.

Based on natural data, first synthesis of diamond in the carbonate-carbon systems were performed in melts-solutions of the $K_2Mg(CO_3)_2$ -C (graphite) systems at 9-10 GPa [2,3] and $Na_2Mg(CO_3)_2$ -C and $Na_2KMg(CO_3)_2$ - C at 7-11 GPa [4]. Thermodynamic and experimental data as well as carbon isotopy data suggested that the carbon source for diamond was graphite but not carbonate [2,3,5]. The processes were therefore interpreted as crystallization of diamond from a carbon solution in an alkali-carbonate melt [3]. i.e., the physicochemical processes of diamond formation in carbonate-carbon systems are similar to the known metal carbonate-carbon synthesis of diamond [6] the mechanism of which was considered in [7,8]. The carbonate-carbon synthesis of diamond differs chemically from the metal-carbon one. The carbon solvent is a carbonate melt, and diamonds which crystallize from carbonate melts-solutions are a novel diamond material in its growth peculiarities and real structure, i.e., in essence, novel synthetic diamonds. The scanning and spectral cathodoluminescence data suggest the conclusion on the similarity of the physical properties of "carbonate-carbon" diamonds with natural nitrogen-free diamonds of type IIa and enable one to establish principally serious differences between diamonds produced by "carbonate-carbon" synthesis on the one hand and by "metal-carbon" on the other one [9,10].

In this work we report on new "carbonate-carbon" syntheses of diamond at 8-10 GPa in the systems: $Na_2Ca(CO_3)_2$-C, $K_2Ca(CO_3)_2$-C, $Li_2Ca(CO_3)_2$-C and $Li_2Mg(CO_3)_2$-C. For the same systems we performed growth of "carbonate-carbon" diamond layers on seed crystals of synthetic "metal ($Ni_{50}Mn_{50}$)-graphite" diamond.

The starting material were $K_2(CO_3)_2$, $Na_2(CO_3)_2$, $Li_2(CO_3)_2$, $CaCO_3$, and $MgCO_3$ agents mixed in stoichiometric ratios yielding the compositions conforming to particular carbonate compounds with mixed alkali and alkali-earth cations: $Na_2Ca(CO_3)_2$, $K_2Ca(CO_3)_2$, $Li_2Ca(CO_3)_2$, and $Li_2Mg(CO_3)_2$. In turn, these stoichiometric mixtures were blended with special-purity graphite (1:1 in weight) . Anvil-with-hole high-pressure apparatuses [11] were used in the runs. The peculiarities of diamond crystallization were studied by SEM (CamScan instrument, Au coating, Dep. of Petrology, Moscow State Univ., operated by E.V.Guseva) under conditions for reflected and secondary electrons. Spontaneous crystallization in alkali-carbonate systems gives rise to full-faceted colorless transparent diamond crystals of octahedral habit plane. The nucleation density is high, crystal intergrown, their nonuniform development are typical. No obtuse smooth cubic {100} faces are observed. The twinning processes evolve by the spinel law-pair-wise intergrowths of twinned crystals, rarely more complicated intergrowths of polysynthetic character are common. Sometimes one can observe pseudocubic rough faces the skin layers of which are formed of closely intergrowth octahedral single crystals, as was found in natural cubic crystals [12] .

The introduction of diamond seed crystals into the runs was ancillary, mainly for testing the boundary between the PT-regions of spontaneous crystallization of diamond (i.e. the region of labile solutions, RLS 8,15]) and, in principle, was not aimed at controlled seed-stimulated diamond growth. Seed single crystals had smooth octahedral {111} and cubic {100} faces which allowed us to study the peculiarities of growth of neogenic layers of carbonate-carbon diamond of faceted forms of differing symmetry. The morphologic peculiarities of carbonate-carbon diamond stimulated seed growth are characterized by the formation of a mosaic smooth surface on octahedral faces and a rough surface on cubic faces, i.e. the way of carbonate-carbon diamond growth is different for octahedral {111} and cubic {100} faces, as first reported by us in [3]. Possibly, these differences in the growth of unlike seed crystal faces reflect the fact that the growth on exclusively octahedral faces is inherent in the carbonate-carbon diamond, at least in the studied systems. One can then assume that this peculiarity is due to chemism of the solvent employed, - alkali-carbonate melt in our case. This effect was observed in natural diamonds of gem quality that also grow in octahedral layers [14] whereas for metal-carbon synthetic diamonds the new layers deposition surface are parallel to the growth faces. Sometimes the history of seed crystals was more complicated when dissolution processes gave way to growth processes. In that case pyramidal growth hills (fig.1a) and a honeycomb texture of negative microcrystals (fig.1b) formed on the dissolved surface. The available observation suggests that the lowest pressure threshold for spontaneous nucleation is inherent in the $Na_2Ca(CO_3)_2$-C and

[#] The work was sponsored by the Federal Program "Integration" (project N 250) and RFBR (Grant N 99-05-65591)

$Li_2Ca(CO_3)_2$-C systems. So, spontaneous crystallization of diamond was first accomplished in alkali-carbonate melts of the $K_2Ca(CO_3)_2$-C, $Na_2Ca(CO_3)_2$-C, $Li_2Ca(CO_3)_2$-C, and $Li_2Mg(CO_3)_2$-C systems at pressures of 8.5-9.5 GPa. The effects of growth of carbonate-carbon diamond layers on single-crystalline seeds were obtained for the first time.

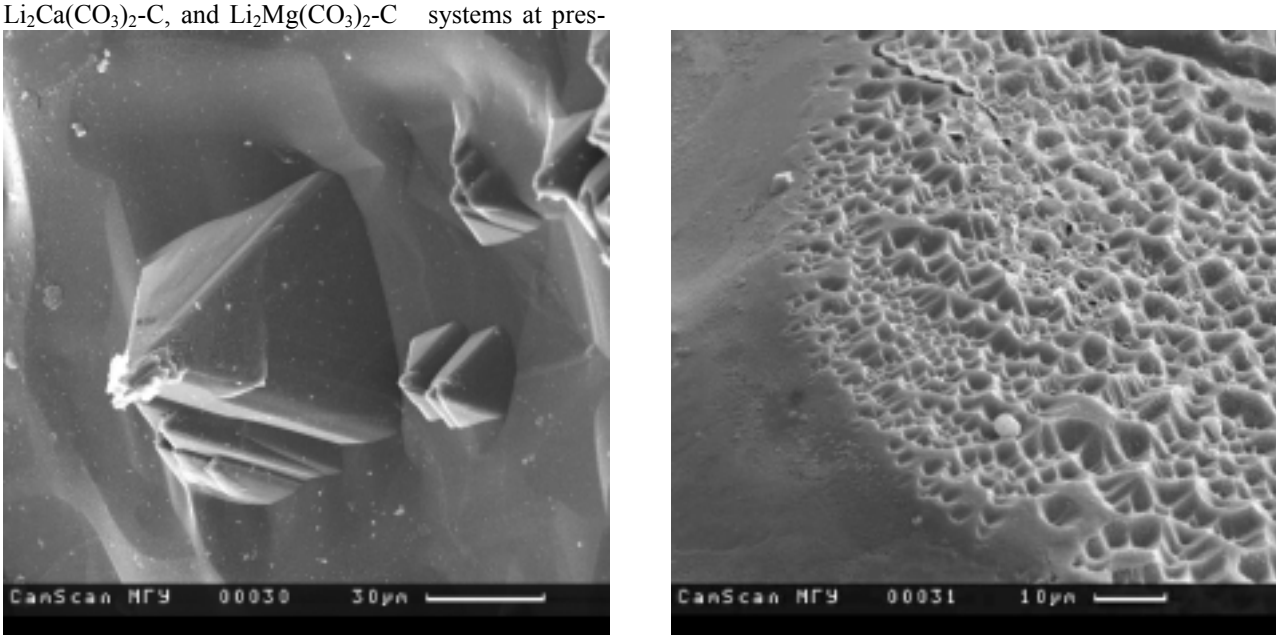

Fig.1. Seed - stimulated diamond growth in the $Na_2Ca(CO_3)_2$ system at 8.5 GPa, 1750°C, 65 min duration (sample 303) a) growth pyramid, b) honeycomb growth texture.

References:

1. Schrauder M., Navon O. (1994) Hydrous and carbonatitic mantle fluids in fibrous diamonds from Jwaneng, Botswana. // Geochim. Cosmochim. Acta, V.58, N2, pp.761 - 771.
2. Taniguchi T., Dobson D., Jones A.P., Rabe R., Milledge H. J. (1996) Synthesis of cubic diamonds in the graphite - magnesium carbonate and graphite - $K_2Mg(CO_3)_2$ systems at high pressure of 9 - 10 GPa region. //J. Mater. Res., V.11, N.10, pp.1 - 11.
3. Litvin Yu.A., Chudinovskikh L.T., , Zharikov V.A. (1997) Experimental crystallization of diamond and graphite from alkali-carbonate melts at 7-11 GPa. // Doklady Ak. Nauk, V.355A, N.6, pp.908-911.
4. Litvin Yu.A., Chudinovskikh L.T., Zharikov V.A. (1998) Crystallization of diamond in the $Na_2Mg(CO_3)_2$-$K_2Mg(CO_3)_2$-C system at 8-10 GPa. // Doklady Earth Sci., V.359A, N.3, pp.433-435.
5. Litvin Yu.A., Chudinovskikh L.T., Zharikov V.A., Shiryaev A.A., Galimov E.M., Saparin G.V., Obyden S.K., Chukichev M.V., Vavilov V.S. (1998).Diamonds of new carbonate - graphite syntheses: crystal growth in the $Na_2Mg(CO_3)_2$ - $K_2Mg(CO_3)_2$ - C system, carbon isotopy, scanning electron microscopy and cathodoluminescence. //Experiment in Geosciences, V.7, N2, pp.48 – 49.
6. Bovenkerk H.P., Bundy F.P., Hall H.T., Strong H.M., Wentorf R.H. (1959) Preparation of diamond. //Nature, V.184, N4693, pp.1094 - 1098 .
7. Litvin Yu.A. (1968) On the mechanism of diamond formation in the metal-carbon systems. // Izv. Akad. Nauk SSSR, Neorg. Mater., N.9, pp.637-639.
8. Litvin Yu.A. (1963) On the problem of diamond genesis. // Zapiski Vsesoyuzn. Min. Obschestva, V.98, N.1, pp.114-121.
9. Litvin Yu.A., Chudinovskikh L.T., Saparin G.V., Obyden S.K., Chukichev M.V., Vavilov V.S. (1998).Peculiarities of diamonds formed in alkaline carbonate - carbon melts at pressures of 8 - 10 GPa: scanning electron microscopy and cathodoluminescence data. // J. Scanning Microscopies, V.20, pp.380 - 388.
10. Litvin Yu.A., Chudinovskikh L.T., Saparin G.V., Obyden S.K., Chukichev M.V., Vavilov V.S. (1998).Diamonds of new carbonate - carbon HP syntheses: SEM morphology, CCL - SEM and CL spectroscopy studies. Diamond and Related Materials, Proceedings Volume of the Diamond - 98 Conference, 13 - 18 September 1998, Hersonisos (Crete), Greece. London: Elsevier .
11. Khvostantsev L.G., Vereshchagin L.F., Novikov A.P. (1977).Device of toroid type for high pressure generation. High Pressure - High Temperature, N.9, pp.637 - 639.
12. Orlov Yu.L. (1963) Morphology of diamond. // M., USSR, Ac.Sci. Press 236 p.
13. Litvin Yu.A., Chudinovskikh L.T., Zharikov V.A. (1998) The growth of diamond on seed crystals in the $Na_2Mg(CO_3)_2$ - $K_2Mg(CO_3)_2$ - C system at 8-10 GPa. // Doklady Earth Sciences, V.359A, N.3, pp.464-466.
14. Shigley J.E., Fritsch E., Stockton C.M., Koivula J.I., Fryer C.W., Kane R.E., Hargett D.R., Welch C.W. (1987) The gemological properties of the De Beers gem - quality synthetic diamonds. Gems Gemol., V.23, N.4, pp187 - 206.
15. Litvin Yu.A., Butuzov V.P. (1972) On the kinetics of diamond growth from metal melt solution. // In: Crystal growth, V.9, M., Nauka Press, p.65-69.

[#]Matveev Yu.A., Chudinovskikh L.T., Litvin Yu.A. Experimental modeling of carbonate-silicate magmatism in connection with genesis of the diamond-bearing rocks from the Kokchetav massif.

key words [*diamond Kokchetav massif experiment carbonate-silicate*]

The discovery of non-kimberlite diamonds in the Kokchetav massif (North Kazakhstan) has brought up to question: what is their genesis?

The manifestations of diamond are found in the Kumdy-Kol' deposit, most in diamond-rich being carbonate-silicate rocks composed of dolomite and silicates mainly represented by clinopyroxene and pyrope-grossularite garnet. A detailed study of these rocks has shown that diamond occurs in the form of inclusions in garnet. together with diamond there are potassium-bearing clinopyroxene and other ultrahigh-pressure minerals [1-4]. These findings have opened up the problem of primary composition and genesis of these rocks.

The recent successful synthesis of diamond from carbonate-graphite systems [5,6] and the finding of potassium-rich and carbonate inclusions in diamonds [7] suggest the idea that diamonds from carbonate-silicate rocks from the Kokchetav formation have magmatic origin. In order to confirm this hypothesis, we have performed an experimental modeling of this process.

The runs were carried out at 70 kbar within the temperature interval 900-2000^{o}C in an anvil-with-hole apparatus with a toroidal sealing KC=K_2CO_3, KMC = $K_2Mg(CO_3)_2$, Di= diopside $CaMgSi_2O_6$, Cros=$Ca_3Al_2Si_3O_{12}$, Wol=wollastonite $CaSiO_3$. The results are listed in Table1.

It has been experimentally found that at high pressure (70 kbar) intensive carbonate-silicate reactions with the participation of a melt occur in the systems studied. It has also been found that crystallization of a carbonate-silicate melt (present in the products, starting at 1200^{o}C, as dendrite-like quenched carbonate and silicate differentiates) gives rise in the near-solidus region to a stable paragenetic association of mineral phases: potassium-bearing clinopyroxene + grossularite - pyrope garnet +Ca-Mg-K-carbonate $\pm$ potassium silicate phases + coesite. This association virtually copies the natural paragenesis of carbonate-silicate rocks with diamond and coesite from the Kokchetav metamorphic formation.

So, we have experimentally confirmed the idea suggested by natural observations that these rocks incorporating ultrahighpressure mineral relicts can be products of crystallization of differentiates of carbonate-silicate melt formed at mantle depths.

[#] The work has been sponsored by the RFBR (Grant N 98-05-64033) and Federal Research Project "Integration" N 250.

Table 1. Run conditions and results.

Run no.	T°C	P, Kbar	Time, min	Run products
$KMC_{50}Di_{25}Gr$				
369	900	70	360	Grt, Di, Carb
178	1000	70	80	Grt, Di, Qz, Carb
155	1200	70	90	Grt, Di, K-Cpx, Carb(K-Ca)
166	1300	70	60	Grt,Di, K-Cpx, Carb
169	1500	70	30	Grt, Di, Qz, Carb
179	1640	70	15	Grt, Di, Carb
365	1900	70	15	Grt, Di, Phl Carb(K-Ca)
367	2000	70	5	Grt,Di, Phl, Carb(K-Ca),Cal
376	1200	50	185	Grt,Di, Phl, Carb(K-Ca),Cal
377	1800	50	30	Grt, Phi, Carb(K-Ca), Cal
$KMC_{50}Wol_{25}Gross_{25}$				
185	1000	70	60	Grt, Di, K-Cpx, Carb
156	1200	70	90	Grt, Di, Carb
184	1600	70	15	Grt, Di, K-Cpx, Qz, Carb
$KC_{50}Di_{25}Gross_{25}$				
265	1110	70	120	Grt, Di, K-Wad, Carb
256	1200	70	60	Grt, Di, Carb
258	1300	70	60	Grt, Di, Carb
259	1400	70	50	Grt, Di, K-Cpx, Carb
264	1500	70	40	Grt, Di, K-Cpx, Carb
268	1600	70	40	Grt, Di, K-Cpx, Carb
267	1710	70	20	Grt, Di, K-Cpx, Carb
$KC_{70}Di_{15}Gross_{15}$				
310	1650	70	60	Grt, Di, K-Cpx, Carb
315	1600	70	180	Grt, Di, Carb

316	1770	70	30	Grt, Di, Carb
$KMC_{30}Di_{35}Gross_{35}$				
375	1890	70	20	Grt, Di, Carb

References:

1. Luth R.W. (1997) Experimental study of the system phlogopite-diopside from 3.5 to 17 GPa. // Am.Mineral., V.82, pp. 1198-1209.
2. Harlow G.E. (1997) K in clinopyroxene at high pressure and temperature: An experimental study. // Am. Mineral., V.82, pp.259-269.
3. Perchuk L.L, Yapaskurt V.O., Okay A. (1995). //Petrology, 3(3), 267-309.
4. PerchukL.L., Yapaskurt V.O. (1998). // Geology and Geophysics, 39 (12), 1756- 1765.
5. Taniguchi T., Dobson D., Jones A.P., Rabe R., Milledge H.J. (1996) Synthesis of cubic diamond in the graphite-magnesium carbonate and graphite-$K_2Mg(C0_3)_2$ systems at high pressure of 9-10 GPa region. // J. Mater. Res., 11(10), 1-11.
6. Litvin YU.A., Chudinovskikh L.T., Zharikov V.A. (1997) Experimental crystallization of diamond and graphite from alkali-carbonate melts at 7-11 GPa. //Doklady of the Russian Academy of Sciences, 355A(6), 908-91.
7. Navon O., Hutcheon I.D., Rossman G.R, Wasserburg G.J. (1988). // Nature, 335, pp.784-789.

Gorbachev N.S., Novikov M.P., Gorbachev P.N. Solubility of sulfur in hydrous silicate melts at high pressures (from the experimental data).

key words [*sulfur solubility magma pressure fluid experiment*]

Introduction. Sulfide-silicate liquation of silicate melts plays an important part in the processes of magmatic differentiation and formation of sulfide ore deposits. In order to understand the conditions of sulfide-silicate liquation one has to know sulfur solubility in magmas under the conditions of sulfide saturation at different P-T-X- parameters. The available data obtained either experimentally or in analysis of homogeneous melt inclusions of igneous rocks characterize sulfur solubility mostly in "dry" silicate melts. Meanwhile, many intrusions with commercial sulfide mineralization and horizons with low-sulfide platinum mineralization in layer massifs contain primary-magmatic amphibole which is indicative of high H_2O pressure at magma crystallization. In order to understand the conditions of water-bearing magmas sulfide saturation, we have studied the solubility of sulfur in hydrous silicate melts in the range of P=1-25 kbar, T=1250-1350^{o}C under the sulfide saturation conditions.

Experimental technique. A piston - cylinder apparatus and a peridotite capsule technique were used in this work. A peridotite capsule loaded with finely ground water-bearing glasses of tholeiite or alkali - olivine basalts and synthetic sulfide of Fe-Ni-Cu was inserted into a ferruginized platinum tube which was welded tight. In the course of the runs the temperature was controlled with a Pt-Pt Rh thermocouple with an accuracy $\pm 5^o$C, the pressure - $\pm$1 kbar. The fugacity of sulfur and oxygen, close to QFMPo buffer, was estimated using reference buffer associations. The run products were studied by optical methods and with a microprobe.

Results. After quenching the sample preserved its initial structure with clear boundaries between the peridotite capsule, silicate glass contained in it and sulfide droplets in the glass and the capsule. The composition of the produced glasses conformed (depending on the P-T-X conditions) to olivine or picrite basalts, from 12 to 22 wt% MgO. The concentration of sulfur in the glasses depending on the P-T-X parameters varied from 0.5 to 2.5 wt % SO_3 which attests to a significant effect of these parameters on solubility. As a whole, the solubility of sulfur in hydrous melts is half an order and more in excess of its solubility in "dry" melts of the same type.

Effect of temperature. A positive linear dependence of sulfur solubility on temperature is observed. At P=15 kbar a temperature increase from 1250 to 1350^{o}C leads to an increase of sulfur solubility by 1.9 times, from 1.37 to 2.58 wt% SO_3. From the data of [1], at P=20 kbar in dry basalt melts sulfur solubility also grows linearly with temperature but the temperature effect dCs/dT=0.4 is smaller than in hydrous melts dCs/dT=1.2 (fig.1).

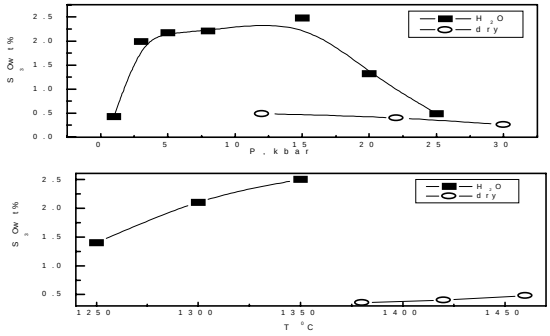

Fig.1. Solubility of sulfur in basalt melts vs temperature.

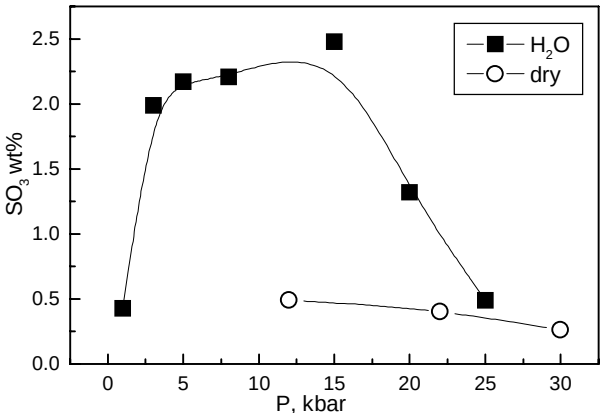

Fig.2. Solubility of sulfur in basalt melts vs pressure. I- with H_2O, T=1350^{o}C, our data; II- "dry", T=1420^{o}C, the data of [1].

Effect of pressure. The pressure dependence of sulfur solubility is of extremal character with the solubility maximum between 10 and 15 kbar. In the range of P=1-10 kbar at T=1250 and 1300°C sulfur solubility increases with pressure from 0.5 to 1.6 wt% of SO_3. At T=1350°C in the range of P=15-25 kbar one can observe the inverse dependence of sulfur solubility on the pressure, as the pressure increased, sulfur solubility decreased from 2.45 at P=15 kbar to 0.5 wt % of SO_3 at P=25 kbar (fig.2.) The negative pressure dependence of sulfur solubility in the range of P=13-30 kbar was also observed in dry basalts melts [1]. Extrapolation to a low pressure region yields an extremely high sulfur solubility, to 1 wt% which is nearly one order of magnitude higher, than solubility in "dry" melts, as suggested by numerous reports. All these attest to extremal behaviour of the pressure dependence of sulfur solubility in hydrous and "dry" magmas with the maximum between 10 and 15 kbar.

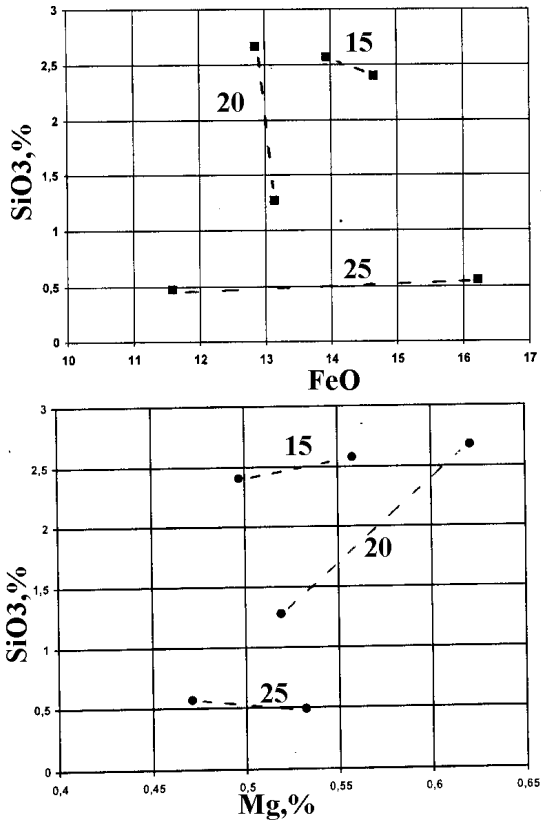

Fig.3.Solubility of sulfur in water-bearing basalts melts as a function of a) FeO concentration; b) magnesiality Mg=MgO/MgO+FeO.

Effect of the melt composition. Sulfur solubility grows with growing FeO concentration in melts. In iron-rich melts (>10wt% FeO) sulfur solubility depends also on melt acidity-basicity, the measure of which can be concentrations of SiO_2 and MgO. Sulfur solubility is maximal in melts with high concentration of MgO and, accordingly, low concentration of SiO_2 (fig.3).

Geological applications. The hydrous magmas have more higher potential ability for forming of the ores to compare with "dry" magmas due to unique ability for dissolve sulfur, chlorine, and ore elements (Cu, Ni, Au, PGE).

Due to high solubility in hydrous melts high sulfur concentrations are called for reaching sulfide saturation, therefore the sulfide-silicate liquation, particularly an early one, is difficult in these melts. At an autonomous evolution of magmatism (without the interaction with crystal rocks) the sulfide saturation can be reached at terminal crystallization stages in residual melts enriched in SiO_2, depleted in FeO and MgO wherein sulfur solubility is minimal. An important factor contributing to the achievement of the water-bearing magmas sulfide saturation can be a change in the chemical composition of magmas - an increase of the sulfur concentration and silicoacidity of the melt, a decrease of its basicity at the reaction-assisted evolution of magmatism due to crystal contamination.

References:

1. Wendlandt R.F. (1992) Sulfide saturation of basalt and andesite melts at high pressures and temperatures. // Am. Mineral., V.67, N.3, pp.877-885.
2. Gorbachev N.S. (1989) Fluid-magma interaction in sulfide-silicate systems. //M., Nauka Press, p.126.
3. Gorbachev N.S. (1990) Fluid-magma interaction in sulfide-silicate systems. // Inter. Geol. Rev., V.32, N.8, pp.749-831.

#Konnikov E.G., Pal'yanova G.A. Solubility of NaCl and HCl in a pyrrhotite melt.

key words [*pyrrhotite melt halite solution hydrochloric acid solidus temperature*]

An investigation of extracts from gas-fluid inclusions in sulfides forming ore veins of Cu-Ni deposits (Farrow et al., 1994) has shown a widespread occurrence of chlorides of various metals. But there are scarcely any data on the effect of chlorine on the thermodynamic properties of sulfide melts wherefrom ore veins crystallize. First clues to the subject were experimentally obtained by N.S.Gorbachev and I.Ya.Nekrasov (1978), but the results obtained by them were questioned by some investigators (Sargsyan et al., 1988). We therefore, attempted to run the experiments in the pyrrhotite -chloride system at the redox potential ensuring an equilibrium of pyrrhotite (Po) and magnetite (Mt) which makes it possible to note the molten phase by the appearance of graphic intergrowths of these minerals in quenching products.

The work was sponsored by the RFBR (Project N 96-05-64714)

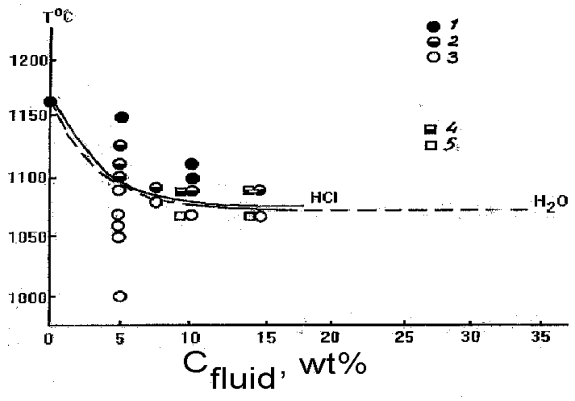

Fig.1. Solidus in the Po+H2O(dash) and Po+HCl (continuous line) systems. Melting: complete (1), partial (2) absent (3) in the presence of 0.5 N HCl solution; partial (4) and absent (5) melting of pyrrhotite with 2N HCk solution.

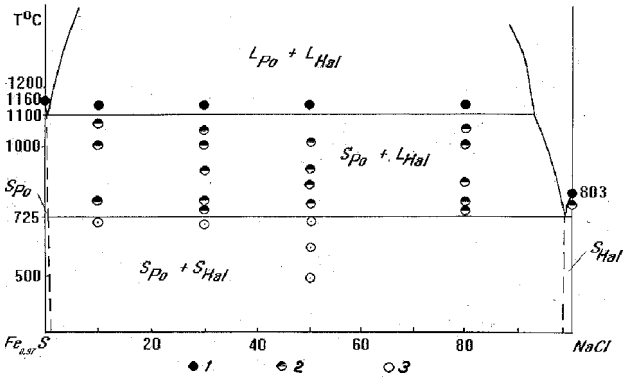

Fig.2. Phase equilibrium diagram for saline Po+Hal system. Symbols: 1- complete melting, 2 - partial melting, 3 - no melting.

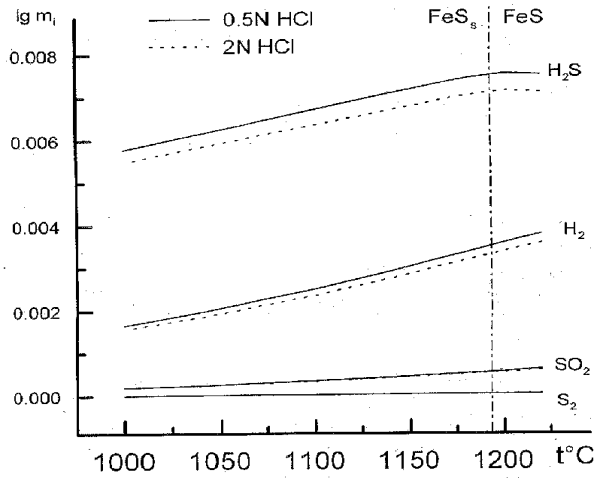

Fig.3. Temperature dependence of the molar fraction of gases formed at melting of pyrrhotite with HCl.

Because of the inability of sulfides to glassify, the effect of chlorine on solubility in a pyrrhotite fluid was estimated from the content of the fluid phase in the system that should provide maximal decrease in the sulfide melt solidus temperature. Two run series were performed in the melt + fluid (Po+H_2O+HCl, 20 runs) and salt ($Fe_{1-x}S$+NaCl, 27 runs) systems. The first series was carried out with 0.5N- and 2N water solutions of HCl in platinum capsules at P=12 kbar, T=1050-1150°C and f_{O2} controlled with a NNO buffer. A capsule-in-capsule technique was employed. The inner capsule contained a pyrrhotite charge and a fluid, the outer one - a buffer mixture (Ni+H_2O). The both capsules were welded. The results of that run series showed that neither the presence of HCl nor the degree of its concentration affect the melting temperature of pyrrhotite: the solidus line of iron monosulfide is the same in the presence of HCl of different concentrations as in the presence of pure water. (fig.1.).

The runs in the salt system were performed in welded preevacuated quartz capsules under normal pressure in a silit furnace (KS-1350/25, made in DDR). The melting temperature range (700-1160°C) was chosen with account taken of the liquidus temperatures of Po and halite (Hal). The phase equilibrium diagram plotted from the experimental results (fig.2) bears witness to nearly complete immiscibility of Po and Hal. As suggested by the X-ray spectral analysis data. in a pyrrhotite melt maximally 1.03 wt% Hal dissolves, and in a Hal melt no more than 0.73 wt% FeS does. The results of these studies are in good agreement with those obtained for a melt - fluid system.

The melting thermodynamics of pyrrhotite under a pressure of a water-hydrochloric fluid was modelled by G.A.Pal'yanova by using I.K.Karpov's computer program "Selector-C"(1981). The calculations show that in the process of the runs at the interaction of HCl+H_2O-fluid with a sulfide melt there form the following gases (in order of decreasing molar quantities): H_2S, H_2, SO_2, S_2, Cl_2 (fig.3.) The latter is not shown in the figure because of a very low molar fraction (10^{-7} mol%). The amount of hydrogen sulfide and hydrogen is strongly dependent on the temperature of the pyrrhotite -fluid interaction, but with the beginning of melting the formation of H_2S practically ceases whereas the fraction of H_2 in the mixture goes on growing. The concentration of these gases decreases noticeably with increasing concentration of HCl in the fluid phase.

The performed calculations also indicate a growth with temperature of fS_2, fO_2 and molar fraction of Mt in the solid interaction products. The latter is also governed by the fluid-to-pyrrhotite ratio, increasing with the fluid fraction.

So, the experiments performed suggest that the solubility of chlorine in a pyrrhotite melt is, practically, absent and is of no effect on its crystallization temperature.

References:

1. Gorbachev N.S., Nekrasov I.Ya. (1978) Specific features of genesis of basic and ultrabasic ore-silicate magmas (from geologic and experimental data). // Syn. of phys.-chem. petrology., iss.VIII., M., Nauka, pp.5-24.
2. Karpov I.K. (1981) Physicochemical computer modeling in geochemistry.// Novosibirsk, Nauka, 247p.
3. Sargsyan G.O., Arutiunyan L.A., Nerasovskii Yu.N., Savchenko A.N. (1988) on the crystallization temperatures of sulfide associations of the Pechenga Cu-Ni ores. // Geol. of ore deposits, V.30, N.2, pp.95-99.
4. Farrow C.E.G., Watkinson D.H., and Jones P.S. (1994) Fluid inclusions in sulfides fronm Northern and South-

ern range Cu-Ni-PGE deposits, Sudbury structure, Ontario. // Econ. Geol., V.89, N.3, pp.647-655.

#Suk N.I. Effect of phosphorus and chlorine on immiscibility of silicate-carbonate systems. Experimental study.

key words [*silicate-carbonate immiscibility experiment]*

Earlier we studied experimentally melt layering and partitioning of some ore elements (REE, Nb, Ta) among immiscible phases in silicate-carbonate systems (albite-carbonate (Na_2CO_3 or Na_2CO_3+$CaCO_3$) and albite-diopside-carbonate) at T-1100°C and P=2kb (Marakushev, Suk, 1998). The runs were conducted in welded platinum tubes in a high-pressure apparatus for 6 h subsequent quenching.

A broad region of layering of the initial melts to two liquids silicate and carbonate ones was found in silicate-carbonate systems.

In this report we present the results of an experimental study of the effect of phosphorus and chlorine on silicate-carbonate melt layering and partitioning of ore metals in silicate-carbonate systems with added chlorides (NaCl) and phosphoric salts ($NaPO_3$).

The salt phase is inhomogeneous in the phosphate-silicate-carbonate systems, it contains segregations of carbonate and phosphate compositions. The phosphate phase possesses herewith a greater efficiency for concentrating REE than the carbonate one and is enriched in these elements. The phosphate melt concentrates primarily REE while Nb and Ta stay in the silicate melt. (table 1). A more efficient concentration by the phosphate phase of light REE (La,Ce) compared to heavy ones (Y) is also observed.

The chloride-silicate-carbonate systems demonstrate separation of carbon-chloride melts from silicate ones. The salt phase forms a layer in the upper sample part and droplets in the silicate melt. The salt liquid is compositionally inhomogeneous and layers to chloride (NaCl with admixtures of Ca and Mg) and carbonate liquid. The salt phase is depleted in ore metals (REE, Nb, Ta) which concentrate in the silicate melt. Some increase in the rare-earth's concentration is, however, observed for the carbonate phases compared to chloride ones (table 2). The NaCl phase does not practically contain any REEs.

So, our experimental studies show a positive effect of phosphorus and negative of chloride on the concentration of ore elements by salt melts in silicate-carbonate systems. This fact finds support in geochemical features of carbonatites, in particular, carbonatites from the Tomtor massif characterized by the occurrence of pyrchlorine, F-apatite, sulphides, and other accessory minerals attesting the presence of additional fluid components (P, F, SO_2, and others).

The work is sponsored by the RFBR (Project N 97-05-64158)

Table 1. Phase compositions (wt%) in layered silicate-carbonate systems with phosphorus (T=1100°C, P=2 kb)

SiO_2	Al_2O_5	MgO	FeO	Na_2O	K_2O	CaO	P_2O_5	La_2O_3	Ce_2O_3	Nb_2O_5	Ta_2O_5	Sum	PHASE
I													
51.95	10.02	3.88	0.07	7.11	0.24	9.39	1.94	0.54	0.9.1	4.41	3.79	94.25	sil. sol.
0.65	0.12	1.20	0.05	21.63	0.16	33.40	5.25	0.58	0.53	0.48	0.33	64.18	carb.phase
1.78	0.03	0.98	0.04	22.81	0.08	29.30	38.35	0.60	0.70	1.18	0.32	96.17	Na-phosph
3.71	0.12	0.18	0.06	3.21	0.07	44.90	33.58	2.68	2.88	1.04	0.13	92.56	Ca-phosph
II													
43.74	0.70	12.61	0.05	8.50	0.21	12.19	2.88	0.02	0.24	6.65	5.29	93.08	sil. sol
0.96	0.01	2.60	0.00	15.89	0.30	33.23	5.31	0.00	0.26	0.37	0.15	59.08	carb.phase
4.99	0.05	0.22	0.05	1.00	0.06	47.13	34.43	3.09	3.88	0.93	0.40	96.23	phos.phase
III													
50.55	10.12	3.31	0.05	8.28	0.17	12.22	1.23	0.28	0.28	3.54	3.37	93.40	sil. sol
1.59	0.15	0.45	0.05	11.40	0.16	34.01	4.10	0.19	0.08	0.29	0.40	52.87	carb.phase
6.89	0.11	0.22	0.02	1.12	0.09	43.97	25.23	2.88	2.69	0.75	0.47	87.44	phos.phase

Table 2. Phase compositions (wt%) in layered silicate-carbonate systems with chlorine (T=1100°C, P=2 kb)

SiO_2	Al_2O_5	MgO	FeO	Na_2O	K_2O	CaO	Cl	La_2O_5	Ce_2O_3	Nb_2O_5	Ta_2O_5	Sum	PHASE
I													
40.21	0.81	10.73	0.22	15.05	0.11	13.51	1.22	0.64	1.44	2.26	1.16	87.36	sil. sol.
0.25	0.01	1.70	0.01	29.23	0.16	18.82	13.90	0.12	0.18	0.02	0.22	64.62	chlor-carb.
0.35	0.04	2.62	0.02	24.03	0.20	16.73	1.34	0.16	0.41	0.09	0.23	46.22	carb. phase
II													
31.57	3.57	1.94	0.03	9.01	0.11	22.13	1.54	2.52	2.73	3.93	4.19	83.27	sil. sol.
0.91	0.10	0.33	0.00	18.46	0.12	34.82	10.19	0.00	0.11	0.00	0.01	65.05	chlor-carb.
0.59	0.15	0.24	0.08	22.08	0.16	28.42	0.90	0.54	0.49	0.00	0.10	53.75	carb. phase
III													
50.84	5.70	8.84	0.21	9.79	0.06	11.05	1.35	1.15	1.41	2.21	1.88	94.49	sil. sol.
0.21	0.03	3.61	0.01	29.83	0.27	22.48	1.33	0.53	0.57	0.00	0.00	58.87	carb. phase
IV													
32.22	4.06	6.26	0.26	2.39	0.04	24.80	0.02	1.10	1.53	1.53	4.90	79.11	sil. sol.
0.27	0.01	0.64	0.00	8.49	0.12	24.56	5.62	0.95	0.85	0.04	0.10	41.65	carb. phase

NaCl phase is present in the samples.

Reference:

1. Marakushev A.A., Suk N.I. (1998) Carbonate-silicate magmatic layering and the problem of the carbonatite genesis. // Dokl. Akad. Nauk, V.360, N.5, pp.681-684.

#Salova T.P., Zavel'sky V.O. Role of sodium in the interaction of a Na-silicate melt with a water fluid (NMR ^{1}H and ^{23}Na)

key words [*water containing glasses Pake's doublet melts NMR-spectra*]

Water containing Na-silicate glasses of the composition $Na_2O{\cdot}3SiO_2$ and $Na_2O{\cdot}4SiO_2$ with different water content were studied by NMR and ^{23}Na methods.
The ^{23}Na spectra obtained at room temperature are a superposition of a wide (S_W) and narrow (S_N) signal (see Table).

The integral intensity ratio of these signals depends on the concentrations of water in the glasses: the intensity of the narrow component grows with growing water content of the glass. The width of the both components grows herewith.

It may be assumed that in a Na-silicate melt a Na^+ ion incorporates into the quartz matrix structure in two ways: 1) with breaking the bridging Si-O-Si bonds and formation of the Si-O-Na form (the covalent bond with O, the wide line in the NMR-spectrum); or 2) by intruding into a recess formed to the type of crown-ethers by bringing oxygens with their unshared electron pairs (non-covalent co-ordination bond, the narrow line in the spectrum).

Inasmuch as the sodium nucleus has a spin 1=3/2, the principal relaxation mechanism of the system of sodium nuclear spins in a strong magnetic field (that dictates the NMR ^{23}Na signal width) is the quadrupole interaction. The intensity of this interaction is governed by the electric field gradient value on the nucleus, i.e. by the symmetry of its electron environment. Clearly, the symmetry of the Na^+ environment in the second case is much higher than in the first one and the ^{23}Na nuclei of the second type from the narrow spectral component. The sodium nuclei in the Si-O-Na bonding form the wide line.

At the interaction of a water fluid with a Na-silicate melt at least some part of water molecules dissociate. A proton (H^+), possessing a higher acidity as compared with a Na^+ ion displaces the latter out of the Si-O-Na to form the Si-OH bond. The displaced Na^+ ion is bound to locate in the oxygen recess thus increasing the narrow component intensity (figs1,2).

The NMR ^{1}H spectra of the glasses being studied are nearly completely identical to the NMR-spectra of albites (1,2) both in form and temperature behaviour. They clearly demonstrate (especially at low temperatures) Pake's doublet (PD), indicating the existence of isolated water molecules in the objects in question, and a wide central line. As the temperature grows, the intensity (and splitting) of the PD in the spectra on glasses under study (as well as in albite spectra) decreases. In the spectra of glasses with high water concentration at temperatures above 300°C one can observe a drastic narrowing of the central line (again, like in albite spectra) (Fig.3).

Comparison of the NMR-spectra of water-containing quartz and Na-silicate glasses suggests that precisely Na^+ ions govern the mechanism of the interaction of a Na-silicate melt with a water fluid. Na^+ ions of the second type, being the co-ordination centers, form water solvates as a result of which there appear in the glass water molecules which do not interact with each other (isolated). These molecules form Pake's doublet in the spectrum.

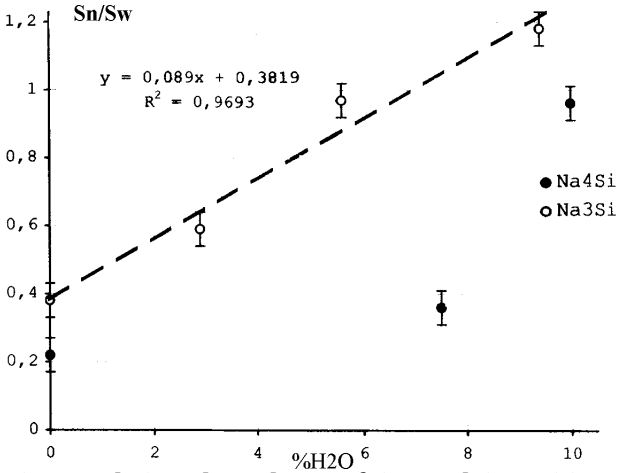

Fig.1. Relation dependence of integral intensities of narrow (Sn) and wide (Sw) lines of ^{23}Na NMR spectra vs water concentrations in glass.

The work has been sponsored by the RFBR (Project N 98-05-64148)

Master table of the NMR ^{23}Na spectra parameters of Na-silicate glasses with different water content.

Parameter	Δ, kHz				S_N/Sw	
	Na3Q		Na4Q		Na3Q	Na4Q
	narrow	wide	narrow	wide	narrow	wide
SiNaDRY	4.5	18.8	4.45	16.6	0.38	0.22
SiNa1	6.8	19.2	5.9	23.6	0.59	0.36
SiNa2	7.4	17.0	6.6	27.4	0.97	0.96
SiNa3	7.7	28.5			1.18	

DRY - water-free samples; SiNa1 - samples with lower water content (Na3Q - 2.9 wt% H_2O, Na4q - 7.5 wt% H_2O); SiNa2 - samples with greater water content ,Na3Q - 5.6 wt% H_2O. Na3Q = $Na_2O{\cdot}3SiO_2$; Na4Q - 10wt% H_2O Na4Q = $Na_2O{\cdot}4SiO_2$), SiNa3 - sample with 0.4 wt% H_2O; S_N and S_W are integral intensities of narrow and wide signal components, respectively, Δ(kHz) is the line width in kHz

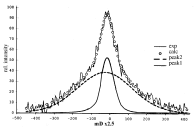

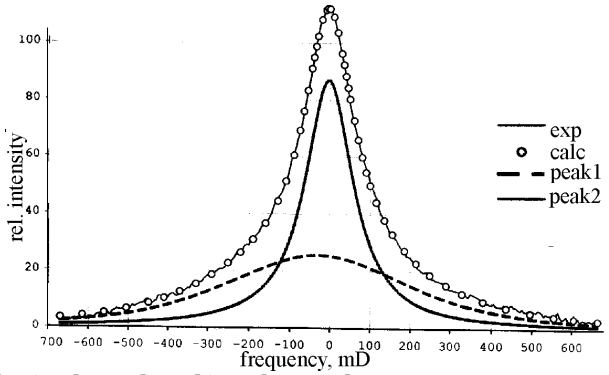

Fig.2. NMR ^{23}Na spectra of a $Na_2O{\cdot}3SiO_2$ sample a) "dry" glass, b) - glass with 9.4 wt%H_2O

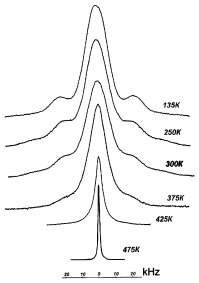

Fig.3. Temperature evolution of the NMR ^1H spectra of $Na_2O{\cdot}3SiO_2$ +9.4wt%H_2O glass.

References:

1. Bartholomew R.F., H.Schreurs W. (1980) Wide-line NMR study of protons in hydrosilicate glasses of different water content.// J. of Non-cryst. solids, V.38-39, pp.679.
2. Zavels'ky V.O., Bezmen N.I. (1990) Water in albite glass (NMR- studies) // Geochim., N.89, pp.1120.

#Kravchuk I.F., Malinin S.D., Senin V.G., Dernov-Pegarev V.F. Solubility of fluorine in hydrous silicate melts.

key words [*melt fluid element partition chlorine fluorine*]

Volatile components in magmatic melts largely dictate the degree of differentiation, crystallization conditions and ore-bearing capacity of a magmatic system. An important role of fluids in the process of hydrothermal ore formation is generally recognized. Most studied is the question concerned with chlorine behaviour at fluid separation from a magmatic melt and its complexing with several ore elements (Cu, W, Pb, Zn) under the magmatic process parameters. Less studied is the role of fluorine-bearing water fluids in equilibrium with aluminosilicate melts. Meanwhile, the data on fluorine content obtained from studies of melt inclusions in magmatic melts of various types vary broadly: from 0.029 wt% in ultrabasic and basic magmas with silicon concentration from 40-53 wt% to 2.087 wt% in acid magmas with silicon concentration more than 64 wt%, topaz rhyolites

The work has been sponsored by the RFBR (Project N 97-05-64881)

and ongonites (Naumov V.B. et al, 1997). These data serve as reference for estimation of possible fluorine concentration in natural melts. Nevertheless, it seems important to obtain direct experimental data on fluorine solubility in acid model melts at strictly fixed temperature and pressure. Table1, borrowed from the review (Carrol, Webster, 1994) presents the published data on fluorine concentration in a melt-fluid system.

Table 1. Fluorine concentration in silicate glass from runs in systems: silicate melt + water phase or water-carbonate fluid + fluoride melt + silicates

Composition of the system	Concentr. of F in silicate glass	Temp. °C.	Pressure, bar	References
granite - LiF-H_2O	< 1*	630-800	980	1
nat. granite - NaF -H_20	< 2**	600-770	980	2
nat. granite HF - H_2O	< 2**	810-820	980	3
nat. granite HF- H_2O	< 3.3*	800	980	4
topaz rhyol. H_20-NaF-AlF_3	< 1-8.5	775-1000	500 - 5000	5
haplogranite H2O - NaF-AlF_3	< 1-6.5	795	2000	6
$NaAlSi_3O_8$ - F_2O_{-1}	18.9	1400	15000	7
$NaAlSi_3O_8$ -NaF-(25% H_2O)	25**	690-850	1000	8
$NaAlSi_3O_8$ -NaF-(50% H_2O)	25**	600-660	4000	8
haplogranite (1-3m HF)	1.17-3.47	750	2000	9

References:
(1) - Gluck et el (1980); (2) - Anfilogov et al (1973); (3) - Gluck and Anfilogov (1973); (4) - Kovalenko (1977); (5) - Webster (1990); (6) - Webster and Holloway (1990); (7) Dingwell (1987); (8) - Koster van Groos and Wyllie (1967); (9) - Keppler and Wyllie (1990).

* The system consisted, possibly, of a silicate melt, fluoride melt and silicate minerals; the runs were conducted with a very high initial fluid-solids ratio in the starting composition. The values for fluorine content in silicate glass were derived by interpolation of experimental data presented in phase diagrams and are therefore rough.

** The values correspond to maximally possible concentrations of fluorine under the given run conditions; nevertheless, the system is characterized by practically complete miscibility between the hydrous albite melt and hydrous williomite melts. The results are seen to have an estimative and nonsystematic character and do not allow one to draw final conclusion about the dependence of fluorine solubility on the melt composition and the fluid composition and concentration.

Table 2. Initial composition of glasses (wt %)

Alumosilicate	K_2O	Na_2O	Al_2O_3	SiO_2	Σ
Ab-Qz	-	6.26±0.50 (15)	11.26±0.40 (15)	82.37±0.30 (15)	99.89
Ab-Ort-Qz	3.78±0.16 (23)	5.70±0.12 (23)	13.22±0.16 (23)	76.25±0.12 (23)	98.95
Ab-Ne	0.2±0.01 (10)	15.36±0.39 (10)	24.58±0.48 (10)	60.41±0.45 (10)	100.37

* In brackets are shown the numbers of analysed sites in the glass samples. The runs were conducted in sealed platinum capsules in a gas bomb at pressures 2-4 kbar and in a piston - cylinder set-up at 6 kbar. The composition of the glasses and the fluorine concentration were defined by an X-ray spectral microanalysis at an accelerating electron voltage 10 kV and probe current 30 nA. In order to minimize the negative factors arising from the probe action on the samples, the measurements were conducted in the scanning mode on an area of 50x50 μm. The reference samples were orthoclase in determining potassium, albite in determining sodium, aluminium, and silicon, fluor-phlogopite for fluorine, chlor-apatite for chlorine determination. The results are illustrated in table 3.

Table 3. Solubility of fluorine in aluminosilicate melts at 850°C.

Run N	Melt composition (l)	Fluid composition (f)	Phase ratio (f:1)	P, kbar	Σ	Concentration of F* (wt %)
1	Ab - Qz	0.5m NaF	1.10	2	92.2	0.40
2	Ab - Qz	1 m NaF	1.03	2	98.S	1.03
3	Ab - Qz	0.5m NaF	0.77	4	89.9	0.33
4	Ab - Qz	1m NaF	1.05	4	87.4	0.88

5	Ab - Qz	1 m NaF	1.12 .	4	89.3	1.13
6	Ab - Ne	0.5 m NaF	0.93	2	89.5	0.62
7	Ab - Ne	0.5 m NaF	1.48	4	90.6	0.40
8	Ab - Ne	1 m NaF	1.13	4	83.3	1.26
9	Ab - Ne	1 m NaP	1.00	4	89.4	1.44
10	Ab- Ort- Qz	0.5 m NaF	1.19	2	88.7	0.68
11	Ab- Ort- Qz	1m NaF	0.86	2	90.9	1.06
12	Ab- Ort- Qz	0.5 m NaF	0.80	4	92.6	0.30
13 .	Ab- Ort- Qz	1m NaF	1.05	4	87.6	1.24
14	Ab- Ort- Qz	0.5m (NaF + NaCl)	1.87	t	92.6	0.59
15	Ab- Ort- Qz	1m (NaF + NaCl)	2.18	2	87.8	0.10
16	Ab- Ort- Qz	0.5m (NaF + NaCl)	1.20	4 •	89.7	0.68
17	Ab- Ort- Qz	1m (NaF + NaCl)	1.44	4	88.7	0.25
18	Ab- Ort- Qz	0.5m NaF+1mNaCl	1.05	4	92.2	0.11
19	Ab- Ort- Qz	1m NaF	0.32	6	91.8	0.89
20	Ab- Ort- Qz	1m Na	0.33	8	97.8	0.46

* The concentrations of fluorine were recalculated to dry glass.

An analysis of these data shows that fluorine incorporates preferentially into the melt and its solubility in the melt increases with increasing fluid concentration in all the systems. The maximum solubility of fluorine in the melts is 1.1-1.5 wt% in agreement with the estimations (Webster, Holloway, 1990). The solubility of fluorine decreases with pressure. The concentration of sodium in the glass after the run is higher than the starting one, but this difference, normally, does not comply with the equivalent concentration of fluorine. The conclusion can whence be drawn about fluorine incorporation into complexing with Al, Si, and Na (Schaller et al, 1992). We have drawn an important conclusion from an analysis of the system with mixed anions (Cl-F), namely, that solubility of fluorine in the presence of chlorine decreases whereas chlorine does not dissolve at all in the melt.

An analysis of the data on ore components partitioning at the interaction of melts with fluorine-bearing fluids suggests that fluoride complexes were not, practically, established for a large number of elements (Cu, Zn, Pb, Mo and W). Fluorine is not a basic component of magmatic fluid phase in many systems. The main cause of this for Ca-bearing systems is low solubility of fluorite and the OH^--for-F^- substitution. Even in the case of magmatic fluids with fluorine, the metal transport is limited due to high stability of SiF_4 complexes.

Bulatov V.K., Girnis A.V. Experimental modeling of heterogeneous mantle melting.

key words [*experiment perodotite melting interaction basalt*]

Partial melting of lherzolite mantle cannot account for some geochemical features of primary basaltic magmas generated under various geodynamic conditions (mid-oceanic rifts, mantle plumes). In particular, the existence of isotopic and geochemical characteristics which indicate that garnet is retained in a restite of basalts from mid-oceanic rifts (Kay, Gust, 1973; Salters, Hart, 1989) contradicts the estimates of the onset of the mantle material melting based on the observable volumes of basaltic magmas (Hirschmann, Stolper, 1996). One of the possible explanations for such contradictions is the presence of garnet pyroxenites or eclogites, along with lherzolites, in the magmas generation zones (Allegre, Turcott, 1986; Hirschmann, Stolper, 1996). This idea is supported by the presence of pyroxenites among mantle noduli. The effect of such heterogeneity on the character of mantle melting and composition of melts was studied experimentally at a pressure 3.5-20kbar and temperature 1250-1400^{o}C.

The samples used consisted of a lherzolite cylinder with a clinopyroxene layer in the central part (table). The mineral compositions in the pyroxenite and lherzolite sample parts were initially identical, that ensured close solidus temperatures of these rocks. In the course of the initial melting the amount of melt in the pyroxenite layer rapidly increases, the reaction melting of clinopyroxene followed by segregation of olivine takes place herewith. The lherzolite zone, about 0.5 mm thick, gets noticeably pyroxene-depleted near the clinopyroxene layers. The 50^{o}C temperature increase from the onset of melting leads to the formation of a molten area surrounded with practically monomineral olivine zone in place of the clinopyroxenite layer. A further temperature increase results in the melt penetration to the lherzolite matrix and showed its homogeneity and similarity with the composition of glasses produced at partial melting of spinel lherzolites close to the total compositions of our samples (Hirose, Kushiro, 1993; Baker, Stolper, 1994) . At the same time an estimation of the melt composition forming upon clinopyroxenite melting indicates that in this case the melts ought to be much more depleted in SiO_2 and enriched in FeO at the identical concentration of MgO, i.e. they should be orthopyroxene-undersaturated. The latter favours high reactability of the melts forming in the course of pyroxenite melting with respect to the surrounding lherzolite which, precisely, gives rise to practically monomineral reaction zones. Our experiments, as applied to melting

processes in the mantle, suggest the following: 1. Clinopyroxenite areas in the mantle can act as melt concentration zones at the initial melting stages. Segregation and accumulation of these melts can efficiently proceed at low total degrees of the heterogeneous mantle melting. 2. In modeling the melting processes of heterogeneous mantle source one has to allow for reactions of the melt, forming in the readily melting part, with high-melting walls. These reactions are capable of rapidly changing the melt composition at the segregation sizes of the order of tens of centimetres. 3. The escape of the melt formed in clinopyroxenite segregations can be regarded as a version for the formation of dunites with rather high iron content similar to noduli carried by basalts generated under different geodynamic conditions.

Table. Chemical compositions (wt%) of rocks used in the runs.

	Series A		Series B	
Component	Lherzolite	Pyroxenite	Lherzolite	Pyroxenite
$Si0_2$	44.5	43.2	45.1	45.7
TiO_2	0.04	0.4	0.05	0.4
$A1_2O_3$	3.12	16.3	3.2	14.2
Cr_2O_3	0.3	2.2	0.3	1.5
FeO	8.8	4.6	8.7	3.8
MgO	40.8	15.9	39.5	15.5
CaO	1.9	15.8	2.8	17.5
Na_20	0.2	1.5	0.3	1.8
Sum	99.66	100	99.95	100

References:

1. Allegre C.J., Turcott D. (1986)// Nature, V.323, pp.123-127.
2. Baker M.B., Stolper E.M. (1994)// Geochim. Cosmochim. Acta, V.58, pp.2811-2827.
3. Hirose K., Kushiro I. (1993)// Earth Planet. Sci. Lett., V.114, pp. 477-489.
4. Hirschmann M.M., Stolper E.M. (1996)// Contrib. Mineral. Petrol., V.124, pp. 185-208.
5. Kay R.W., Gust P.W. (1973)// J. GeoL, V.81, pp. 653-682.
6. Salters V.J.M., Hart S.R. (1989)// Nature, V.342, pp.420-422.

[#]Bolykhovskaya S.V. Computer-modeling of the formation of the Joko-Dovyren layered intrusion.

key words [computer modeling layered intrusion]

Forward modeling of solidification of basite-hyperbasite layered intrusion Joko-Dovyren (North Transbaikalia) has been performed in terms of the COMAGMAT program (Ariskin et al, 1993) realizing a convection-cumulation crystallization differentiation mechanism.

The massif is a substratum body of about 300 m in thickness, characterized by a picrite composition of the original magma. Based on the exchange of cumulative parageneses in the intrusion section, the following zones have been distinguished (from base forwards top): olivine-chromite cumulate zone (Ol+Cr), olivine-plagioclase-chromite cumulate zone (Ol+Pl+Cr), plagioclase-augite-olivine cumulate zone (Ol+Pl+Aug) (Fig.1). Optimal model parameters have been defined at which the naturally observable minerals and components partitionings in the vertical massif section are reproduced most accurately (table 1). The model partitionings were compared with the ten-fold-smoothed natural partitionings of oxides and minerals in the section (Figs. 1 and 2) . The modeling was performed for a closed system under "dry " conditions.

It has been found that the optimal model reflective of the properties of real object accurately enough can be constructed only with the presence in the magma of a considerable fraction of intratelluric impregnations.

Estimations have been carried out in the range of the original magma crystallinity (Fint) from 0 to 60 vol% to show that as the fraction of the intratelluric phases increases at the moment of introduction, the time period for the intrusion formation increases by one order, the ratios along the regions of differing phase composition change. The shortening of the magmatic melt solidification duration is attributed to the fact that a greater part of heat lost thereat is the latent heat of crystallization of which a store is the less the higher is the crystallinity degree of the intruded magma.

In order to obtain the independent estimate of the Fint we have conducted "inverse" modeling by a method of geo-

[#] The work has been sponsored by the RFBR (Project N 99-05-65118)

chemical thermometry (Frenckel et al, 1987) of intrusion rocks from the lower near-contact zone. We have failed to obtain unambiguous results because the evolution lines lacked pronounced "intersections" and "convergences". It is, however, demonstrative that from these data the degree of the initial magma crystallinity ought to be in excess of 60% which is even higher than it has been obtained in the optimal model.

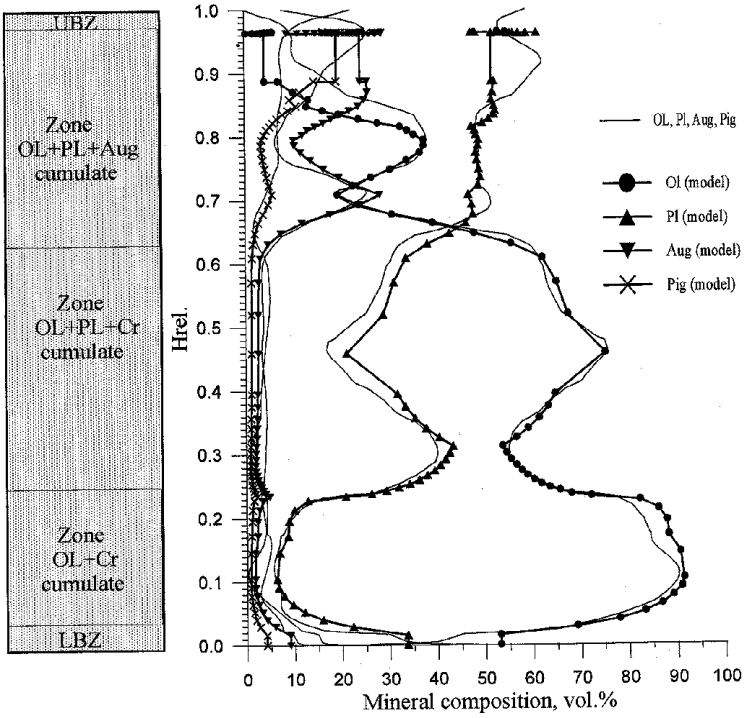

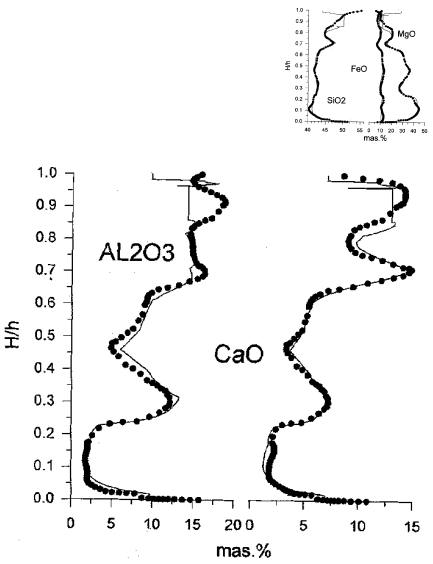

Fig.1. Comparison of the observable and model partitionings of minerals in the intrusion section.

Fig.2. Comparison of model and natural componental partitioning in the intrusion section. The real compositions are shown in filled circles.

The mineral partitioning in the vertical intrusion section is a consequence of balance between solid-state flows into the magma resultant from crystallization and flows out of the magma into a cumulus due to precipitation of particles. The Fint parameter affects the substance flow from magma to cumulus at the initial crystallization stage. In the optimal intrusion mode; it determines the near-contact zone thickness and the position in the vertical section of the boundary between the Ol+Cr cumulates zone and that with the Ol+Pl+Cr cumulative paragenesis. The dynamics of the solid phase introduction into the magma is governed by the rates of heat loss through the intrusion top, and the heat flow through the lower contact governs the velocity of the lower cumulus boundary. These flows are determined by external parameters: heat capacity, thermal conductivity of host rocks, temperature at the upper crystallization from (T_o). It has been shown that of greater effect on the spatial and temporal structure of the process is the model preset parameter DT-the temperature difference between the magma and host rocks on the moment of introduction, determining the T_o value.

The constructed model reproduces the partitioning of petrogenic elements with high accuracy (figs 1,2). This suggests the conclusion of the decisive role of the differentiation process due to crystal precipitation in ten convecting magma in the formation of the geochemical structure of the Joko-Dovyren intrusion.

Table 1. **Parameters of optimal dynamic model.**

Intrusion thickness (H), m	2950
Pressure (P), kbar	1
Fraction of intratelluric phases at the moment of incorporation (Fint), vol.%	44
Temperature difference at the external crystallization front at the moment of incorporation (DT), ^oC	1200
Ultimate cumulus density at the lower crystallization front, vol%	90
Precipitation rates of minerals, m/y:	
olivine	2-0.07
plagioclase	0.37-0.06
augite	1.6-0.2

References:

1. Ariskin A.A., Barmina G.S., Frenkel M.Ya., Nielsen R.L. (1993) COMAGMAT: a Fortran program to model magma differentiation processes. // Computers and Geosciences, V.19, pp.1155-1170.
2. Frenkel M.Ya, Ariskin A.A., Barmina G.S., Korina M.I., Koptev-Dvornikov E.V. (1987) Geochemical thermometry of magmatic rocks - principles of the method and examples of application. // Geochim. N.11, pp.1546-1562.

[#]Lebedev E.B., Kadik A.A., Kuskov O.L., Dorfman A.M., Lukanin O.A. Experimental study on the sulfide phase migration in the partly melted silicate substance: application to the proiblem of planetary core formation

key words *[experiment magmatism centrifuging layered intrusions iron fractionation sulfides the core of the Earth and the Moon]*

At early stages of planetary bodies formation silicate, metallic, and sulfide phases, forming at partial or complete melting of the original planetary substance, underwent gravitational differentiation. Gravitational differentiation is related to separation of crystalline and molten phases in density and composition. It involves concentrational, thermal and phase convection whose proceeding mechanisms are quite complicated.

These processes are supposed to result in formation of the cores and outer shells of the Earth planets and the Moon. For the Moon the question of whether its core is metallic or sulfide is still open. Its solution is of principle importance for understanding the mechanism of the Moon formation and evolution (Galimov, 1995).

A method of high-temperature centrifuging (Lebedev, Kadik, 1998) was first employed to model the processes of accumulation and migration of sulfide phases at partial melting of model planetary substance. The runs suggest that segregation of the sulfide phases and their migration in the intercrystalline space are in close dependence on the mantle melting degree. The results of the studies suggest the following conclusions.

It has been shown that a mixture consisting of olivine crystals, a silicate basalt melt, and a sulfide melt is - density-differentiated when subjected to centrifuging. As a result the iron-sulfide and silicate phases segregate to individual layers.

In sample SC-8 (67.5 vol.% 01, 22.5 vol.% Bas, 10 vol. % FesS) containing -*23* vol.% silicate melt centrifuging produces a drastically nonuniform phase distribution for vertical extension (fig.1). Four major zones are distinguished in the vertical sample section. The upper zone (A) of [v] the ascended basalt melt, represented by glass and quenched pyroxene crystals. It is free of olivine crystals and sulfide globules. The thickness of the upper melt layer is about 2 mm. The transition zone (B). The central zone (C), making up the basic sample part ("6.5 mm in height) contains, largely, olivine crystals, 85-90 vol.% (crystal matrix) and a silicate melt, (glass) 10-15 % occurring in intergranular channels. The width of the intergranular channels is 3-30 μm. In the lower part of this zone in basalt glass, normally in central channel parts, there are small sulfide globules to one micron in size. The amount of sulfide n this zone does not exceed 1-3 vol.%. The phase distribution vertical extension within this zone varies somewhat (fig.2). From the top downwards the amount of the intergranular basalt melt decreases whereas the amounts and sulfide globules increase. Between the upper (A) and the central zone (C) there is a narrow transition zone (B) wherein a drastic olivine crystals-for-basalt melt substitution takes place. The lower bottom zone (D) (-1 mm in height) consists of 100% iron sulfide- pyrrhotine formed from sulfide liquid on the moment of sample quenching.

The observable pattern of the phase distribution for vertical extension in sample SC-8 clearly demonstrates the result of gravitational differentiation o£ substance - phase layering with respect to density. Under the action of gravity the sulfide phase easily percolates (filter) through the crystal matrix via intergranular channels and, over the run time period, practically completely accumulates in the lower sample part.

In the central part there remains only a small fraction of sulfide in the form of tiny globules (droplets) which have had no time to precipitate. Apparently, simultaneously, the silicate liquid percolates in the opposite direction, i.e. to the upper sample part where it forms a pure melt layer.

The occurrence of basalt melt in amounts exceeding 5-10% among olivine crystals is sufficient for the formation of the system of interconnected intergranular channels which become permeable both for silicate and sulfide liquids. Sulfide droplets (globules) do not mix with the silicate melt and are capable of moving via the intergranular melt channels in the process of mixture fractionation. If the amount of silicate melt is less than 5-10%, sulfide droplets are uniformly distributed over the sample (matrix) volume and no sulfide phase motion is observed in the gravity field.

The modeling of chemical differentiation processes of planetary bodies and of core formation in thermal and gravity fields due to the formation of the system of interconnected intergranular channels permeable for both silicate liquid and sulfide melt is substantial contribution in support of a strong melting of upper Moon shells (magma ocean-more than 10-20 % melt) and partial melting of the lower mantle (5-10 melt) at an early stage of evolution of our satellite. Conclusions:

1. It has been shown that a mixture of olivine crystals, silicate basalt melt and sulfide melt differentiates with respect to density when subjected to centrifuging. As a result, the iron-sulfide and the silicate phases are segregated to independent layers.

2. The presence of silicate basalt melt in amounts exceeding 5-10% is sufficient for the arising of olivine matrix permeability both for the silicate and sulfide liquids. If the amount of the silicate melt is less than 5-10%, no sulfide phase intergranular migration is observed.

[#] The work has been supported by the RFBR (Projects N 97-05-64786,98-05-64768, 99-05-65479)

3. Modeling of the chemical differentiation processes of planetary bodies and the core formation in thermal and gravity fields fairly supports the arguments for a significant melting of the upper Moon

shells.

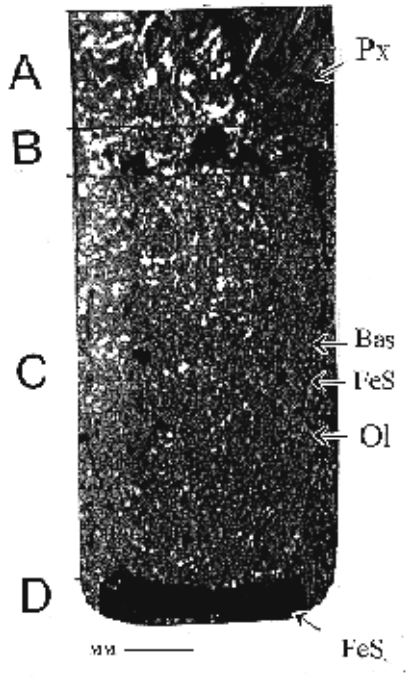

Fig.1. Phase distribution in the sample for vertical extension after centrifuging the mixture: 67.5 vol.% 01; 22.5 vol. % Bas; 10 vol. % FeS. Run SC-8. T=1400°C, acceleration 4000 g; centrifuging time-period 15 min. Vertical cut of the sample of radial extension 9.6 mm. The micrograph of a transparent section (magnification xl5). A- zone of the top accumulated basalt melt sample; B - transition zone, C-central zone (silicate matrix (01+Bas) , in the lower part with sulfide globules, FeS) , D - zone of accumulated sulfide melt.

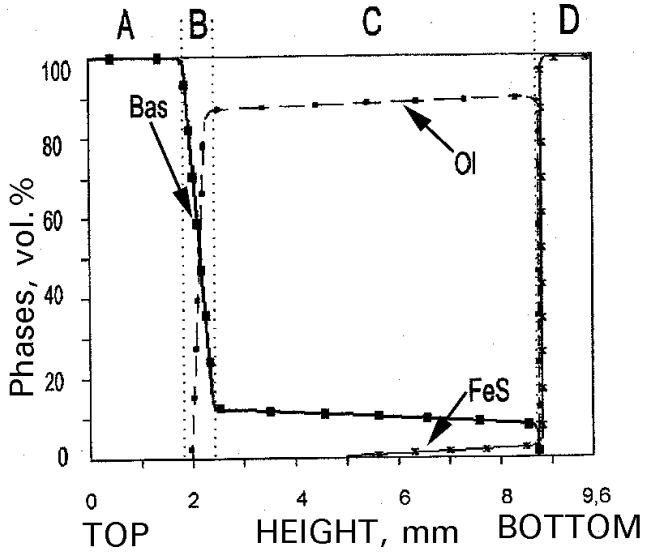

Fig.2. Quantitative phase distribution for vertical extension after centrifuging the mixture: 67.5 vol.% Ol; 22.5 vol% Bas; 10 vol% FeS. Run SC-8. For the run conditions see in fig.1. Ol=-olivine, Bas-basalt melt (quenched glass), FeS - sulfide melt (quenched pyrrhotine). A,B,C,D- the sample's zones, like in fig.1.

References:

1. Galimov E.M. (1995) Problem of the Moon's origin // Principal trends in geochemistry. Dedicated to the 100-th aniversary of A.P.Vinogradov's birth. (Edit. Glalimov E.M.), M., Nauka press, p.8-43.
2. Lebedev E.B., Kadik A.A.???

Mikhailov M.Yu., Shvedenkov G.Yu. Behaviour of water at decompression of saturated melts in the albite-K-feldspar-quartz system.

key words [*silicate melt water decompression*]

We have studied experimentally the behaviour of water in the process of isothermal decompression of the melt of the composition: albite-40.6, K-feldspar - 24.1, quartz - 35.3 wt% in the range from the saturation parameters (P=1000 bar, T=870°C) to final pressures of 400 bar. The duration at decompression varied from 3 minutes to 5 hours. The runs were conducted under the open system conditions with respect to water and silica. The platinum capsules were not welded but only tightly closed and placed into a container filled with finely ground quartz. The ground quartz reduced a loss of the charge material as a result of hydrolysis. Besides, it was believed that the interaction of the silica-saturated fluid and the melt contributed to the fact that by the beginning of decompression the parameters of the melt state closely corresponded to the liquidus surface and even at a small decompression came to the subliquidus region. In order to exclude the appearance of buried water bubbles in the end products, the temperature and pressure were raised in such a way that by the moment of melting the amount of water among the glass grains be wittingly smaller than that required for melt saturation. The melt was with saturated water for 48h. Decompression was done at a rate 50 bar/s. After holding at a decreased pressure, we conducted an isobaric "quenching" at a rate 150-100 deg/min. In order to remove foreign gases the details of the cell and the water were preliminarily boiled for a long time.

Transparent crystal-free glasses with gas bubbles of maximal size not exceeding 5-15 μm were produced in the runs. The gas bubbles concentration was 10^7-10^8 cm^{-3}.

The contents of molecular and hydroxyl water in quenched glasses were defined by the NMR methods. It was found that 1) the concentration of water in glasses produced as a result of isobaric quenching starting with the saturation parameters corresponded to an equilibrium concentration; 2) the concentration of water in glasses produced by quenching the melts subjected to decompression exceed appreciably an equilibrium concentration, 3) the concentrations of molecular and hydroxyl water grow in accordance with Stolper's diagram [1], and in the ratio of the two water forms and water total concentration "decompression" glasses comply with those produced at higher pressures than those in the runs (table).

Table. Results of melt decompression runs in the albite-K-feldspar-quartz system

N order	Decompr. , bar	Holding time after de-compr., S	Concentration of H_2O in glass, wt %			Relative changes in glass density
			Sum	Molec..	Hydroxyl	
1	40	182	3.85	1.89	1.96	-0.30
2	40	625	3.80	1.94	1.86	-0.05
3	40	1460	5.16	2.89	2.27	-0.16
4	100	720	4.09	1.96	2.13	-0.26
5	160	610	4.68	2.38	2.3	-0.30
6	200	18600	4.70	2.41	2.29	-0.36
7	300	960	4.06	1.82	2.24	-0.23
8	500	1200	4.24	2.32	1.92	-0.36
9	500	1200	6.65	4.24	2.41	-0.41
10*	0	0	3.47	1.73	1.74	0

- reference glass at relative density measurement (absolute density of glass is 2.192 ± 0.003 g/cm^3)

The amount of free water in bubbles was estimated by three techniques: 1) from the results of measurements of the number, sizes and filling coefficient of vacuoles in ground sections under a microscope; 2) from the results of determination of a relative density alteration (table); 3) by comparing IR transmission spectra in the wavelength range of 1.7-2.6μm obtained at sample cooling down to -196°C and subsequent heating. Always it was found that the greater part of molecular water in the studied glasses is bound and only 0.3 wt% of the total content is a free water phase in bubbles.

The obtained results show that under the conditions of the open system simulated in our runs an anomalous behaviour of water takes place, namely, in the process of decompression, at least at its certain stage the melt absorbs a volatile component instead of releasing it, and its concentration in the end products appears greater than in the initial melt.

Structural inhomogeneities (e.g. of liquid microimmiscibility structure type) not found in glasses subjected to isobaric quenching without decompression were revealed in "decompression" glasses by structural etching techniques. It is assumed that precisely these inhomogeneities are responsible for the anomalous behaviour of water in melts under our run conditions.

Reference:

1. Stolper E. (1982) // Contrib. To Mineral. And Petrol. V.81, pp.1-17.

Shchekina T.I., Gramenitsky E.N., Batanova A.M., Kurbyko T.A. Experimental simulation of the granite melt-rock interaction.

key words [*interaction zoning substitution granite melt simulation*]

The interaction of a model granite melt with rocks of different basicity - olivine pyroxenite, epidote amphibolite, quartz-normalized dolerite, and garnet-quartz-chlorine-muscovite schist- has been studied in order to understand the mechanism of this process. The runs were performed at 800°C and 1000 bar under the conditions where the system is saturated in water ("hydrothermal") and at 1150°C under normal pressure ("dry").

At every interaction the reaction region gains zoned structure, and in the endocontact the starting granite melt changes its composition getting contaminated in the components of the rock being in contact. Depending on the rock there forms reaction zoning of two types in the exocontact.

The first type is characterized by preferentially metasomatic substitutions of the crystalline rock. The runs conducted under dry and hydrothermal conditions with a monoclinic olivine pyroxenite sample can serve as examples.

In the hydrothermal run the main minerals (orthopyroxene, olivine, a small quantity of plagioclase) remain unchanged while in the dry one olivine drastically reduces its iron content, partly being substituted by an aggregate of orthopyroxene and magnesioferrite.

In either case a contact zone about 10 μm wide is observed where olivine is substituted by orthopyroxene. In "dry" run disseminated magnesioferrite in olivine disappears contactward. The scale of the interaction is one order smaller than the pyroxenite grain size, and the interaction is, actually, not with the rock as a whole but with individual grains. The glass composition is not equal along the contact, it alters as dictated by the composition of the mineral which reacts with granite melt. Near to pyroxene within 7 μm the glass demonstrates increased concentrations of FeO and lowest concentrations of SiO_2 and Al_2O_3. At the contact with plagioclase the concentrations of Al_2O_3 in glass increase by 2-4%, those of CaO increase by 0.2%, and of SiO_2 decrease by 3-5%. With distance from the contact the alterations in glass are more moderate. A part of the reaction glass formed due to dissolution of the adjoining crystal grain, i.e. there are "exo"- and "endocontact" zones (table, schemes 1,2). The latter can be revealed by small but stable concentrations of FeO, MgO, and CaO which decrease gradually with distance from the contact ("contamination" with pyroxenite components).

The second interaction type is characterized by the appearance of an interstitial melt in the endocontact zone. This type encompasses columns produced in a largest number of the conducted runs. They should however be subdivided into two groups.

1. The formation of melt in rocks proceeds by the substitution mechanism due to diffusive gain of components

from the granite melt region and the counter loss of the material from the rock. In this group are the runs with amphibolite under dry and hydrothermal conditions (table, schemes 3,4).

In the hydrothermal run beyond the granite melt interaction region hornblende and plagioclase stay unaltered, and on primary epidote basic (An_{80}) plagioclase evolves. Nearer to the contact between the grains there appear glass rims, and differently, oriented biotite platelets grow on hornblende. In the immediate contact biotite and hornblende disappear, and corroded grains of plagioclase get cemented with glass. Plagioclase acquires herewith a zoned structure with the rims of the basic composition (An_{54} envelopes An_{25} nuclei).

N	Run conditions	Granite melt	Reaction zones				Rock
		endozones		exozones			
1	1150°C, 1 atm 6 h Thickness	L_o	L_1 150	L_2 10	Opx+Pl 15	Opx+Pl+Ol 50	Opx+Pl+Ol+ Mf
2	800°C , P_{H2O}=1 kbar, 167 h Thickness	L_o	L_1 100	L_2 5	Opx+Pl 7		Opx+Pl+Ol
3	1150°C, 1 atm 6 h Thickness	L_o	L_1 ~700	L_2 50	L_2+Cpx 40	L_2+Cpx+ Mf ~!000	Pl+Cpx+Hb? +Mf+Ol
4	800°C , P_{H2O}=1 kbar, 772 h Thickness	L_o	L_1 ~100	L_2 20	L_2+Pl 20	L_2+Pl+Hb +Bi ~300	Pl+Hb
5	800°C , P_{H2O}=1 kbar, 772 h Thickness	L_o	L_1 ~200	L_2 ~150	L_2+ Q ~50	L_2+Q +Cor ~300	L_2+Q+Cor +Gr? ~600	L_3+Q+Cor+ Sill?+Gr+Il m+Mt+Ap

Note: L_o-granite melt; L_1 - contaminated granite melt; L_2 - melt formed at the expense of the rock; L_3- anatexic melt. The thickness is given in mkm. 1 and 2 - runs with olivine pyroxenite, 3 and 4 - with amphibolite; 5 - with garnet-quartz-chlorine-muscovite schist.

The starting phase composition altered appreciably in the course of the dry run (irrespective of granite melt action): hornblende and epidote decompressed completely to clinopyroxene (of the augite composition), magnesioferrite with a subordinate amount of some other ore minerals, basic plagioclase, magnesial olivine. Possibly, there are glass regions in this aggregate. In this case the interaction pertains to the type considered below. Crystal phases consequently disappear in the reaction zones, and the quantity of glass grows. The last to dissolve are magnesioferrite (this substitution front is most pronounced because of the contrast in the phases composition) and then clinopyroxene. In either case, in the near-contact region glass differs compositionally from granite by decreasing concentration of SiO_2 and increasing concentration of CaO, FeO. The site of the most dramatic change in their concentration separated endo- and exozones.

2. Melt forms in a rock not only by the first mechanism but also through its partial melting (anatesis) at run temperatures. Granite melt interacts in this case not with solid but with partly molten rock. In this group are the columns obtained in hydrothermal runs with ground dolerite and garnet-quartz-chlorite-muscovite schist and in dry runs with all rocks but pyroxenite.

As an example, we shall consider the case of the interaction conditions where anatexic melting of the starting rock was most complete. In this run there took place the interaction of two melts, in one of which, formed in schist, both neogenic and relic phases of the primary rock were present.

Partial schist melting gave rise in the rock to glass (10-20%) and cordierite (15-20%), the latter forming preferentially on layered silicates. Of the initial rock minerals there retained quartz (~20%), qarnet, ilmenite, apatite, magnetite. The glass composition is quite homogeneous, conforming to plumasite essentially K-granite. The phase qualitative and quantitative composition of the extreme zone from the interaction run is slightly different from the results of the special run conducted with schist under identical conditions but without granite melt. Nevertheless, the phase aggregates which succeed to the form and some features of the inherent structure of primary chlorine and muscovite advanced noticeably in recrystallization compared to the dummy run. On the strength of this, their overall composition, while keeping high concentrations of iron and aluminium characteristic of these minerals, contains large amounts of silica and alkali oxides due to the presence of a larger amount of glass. Cordierite is represented by idiomorphic crystals of rectangular or hexagonal sections. In dummy run products the crystals are zoned, the iron content in them grows from 40 to 63% towards the edges. Their nucleation occurred, possibly, at the chlorite - muscovite contact the summary composition of which was more magnesial than the total rock composition. Its homogenization in all the system's sites caused an increase in the iron content of cordierite and the appearance of a melt in association with it. In the interaction run cordierite is nonzoned and its iron content is 55%.

The zoning formed at the rock-granite melt contact is not contrast. Nearer to the contact there disappear ore and

subsidary (garnet and, possibly, sillimanite) minerals well seen on reflected-electron images, the amount of glass grows. Quartz grain size is seen to decrease: in sites most distal from the contact it is mostly 100μm, in the middle less than 50μm, in the vicinity of the contact with the granite glass less then 20 μm.

In the sites most distal from the contact the ferruginosity factor decreases to 45%. In the immediate contact with the homogeneous melt the only crystalline phase is quartz. The above mentioned observations make it possible to set the zoning structure for this case (table, scheme 5).

Conclusions.

1. Reaction columns possessing most important properties of metasomatic zoning form at the melt-rock boundary.

2. Melt forms in rocks by the substitution mechanism, as a result of diffusive gain and loss of the material.

Genshaft Yu.S., Tsel'movich V.A., Melt-crystallization in the systems ilmenite-silicate under high pressures.

key words [*picroilmenite experimental modeling high pressure crystallization basalt kimberlite peridotite*]

Magnesial ilmenite (picroilmenite) is an abundant mineral from deep-seated rocks of the earth crust and upper mantle, specifically iron- and titanium-rich, and is encountered among megacrystals in alkali basalts and kimberlites. This circumstance has suggested to many researches the conclusion that the concentration of magnesium in picroilmenite can be a peculiar geobarometers as it increases with pressure of mineral crystallization [1,2].

There are, however, controversial published data on various factors affecting the composition of picroilmenite, especially its magnesiality: temperature [3], bulk melt composition wherefrom picroilmenite crystallized [4,6], oxygen fugacity [6]. In order to study this problem in more detail, the authors have carried out a study of the ilmenite crystallization from iron-and titanium-rich silicate systems of differing composition, primarily differing magnesiality, silico-acidity, alkalinity, under elevated pressures and temperatures. The starting samples were produced in the form of carefully ground powder mixture consisting in mass of 20% natural picroilmenite and 80% rock (picrite basalt N349 from Iceland, basalt N879 from Mongolia, kimberlites -arbonatized N US-207-731 and N OL-R-52 from Yakutia, garnet peridotite xenolite N P360 were used). Chemical compositions of these mixture components are listed in Table 1.

Table 1. **Chemical compositions (wt%) of the starting samples.**

Sample	349	879	OL-R-52	US-207-738	P360	1878
SiO_2	47.12	46.53	37.22	26.56	42.56	-
TiO_2	0.92	2.61	0.09	1.24	0.12	54.1
Al_2O_3	15.35	16.17	1.37	3.39	1.33	0.7
Fe_2O_3	2.55	-	0.14	1.82	0.58	-
FeO	7.46	-	5.67	2.8	8.92	-
MnO	0.17	0.15	0.12	0.05	0.13	0.2
MgO	10.95	4.46	40.19	22.09	44.25	11
CaO	13.92	6.33	1.72	16.04	0.67	0.01
Na_2O	1.22	4.21	0.07	0.4	0.18	-
K_2O	0.05	5.02	0.14	1.72	0.14	-
P_2O_5	0.05	1.4	0.23	0.65	0.06	-
CO_2	-	-	2.47	12.3	0.22	-
H_2O+	0.13	-	8	6.62	0.2	-
H_2O-	0.04	-	1.02	2.96	-	-
FeO*	9.76	10.33	6.43	4.44	9.44	36.1
Cr_2O_3	0.12	0.03	0.055	0.28	0.27	0.03
sum	100.05	97.24	98.51	98.92	99.63	102.14

Note: FeO* - all iron as FeO

The runs were performed in anvil-with-hole and toroid type apparatuses at pressures 15-50 kbar and temperatures to 1500°C, the preset melt crystallization temperature was approached from "top" and "bottom" by a temperature quenching method [7]. Graphite and platinum capsules enclosing initial mixtures were used. In either case under identical run conditions close results for mineral phases crystallization were obtained. In these reaction cells various authors estimate oxygen fugacity to be close to buffer NNO and QFM conditions. The exposure at the given PT-conditions ranged from 20 to 60 min depending on the crystallization temperature.

Below is given a brief characterization of the starting samples.

Sample 349 - vitreous picritobasalt from neovolcanic zone of Iceland, contains phenocrysts of magnesial olivine, chromdiopside, Ca-plagioclase and a tiny amount of chromspinel and titanomagnetite.

Sample 879 - basanite from Holocene volcano of the Hangai mountain in Mongolia. Contains phenocrysts of olivine, clynopyroxene, plagioclase, a large amount of

titanomagnetite and hemoilmenite. The basalt shows up a high concentration of potassium oxide and total high alkalinity.

Sample R 360-inclusion of garnet peridotite from the Yakitian kimberlite, characterized by a small degree of mineral paragenesis alteration (garnet kepyhitization alone is observed) and a high concentration of magnesium oxide. Assigned to a depleted upper mantle substance in petrochemistry.

Sample US-207-731 -carbonatized kimberlite from the Udachnaya pipe West Yakutia, contains micrograins of picroilmenite, spinel, and titanomagnetite.

Sample OL-R-52 - low-carbonatized, serpentized kimberlite from the Ruslovaya pipe, Kuoy field, Yakutia. No optically diagnosed ferrimagnetic fraction is contained.

Sample 1878 - picroilmenite, grains to several mm in size were selected from alluvium of one kimberlite pipe, Jakutia. Demonstrate persistent composition (on average 38 mol% geikielite and 7 mol% hematite in solid solution).

With the exclusion of kimberlite US-207-731, all the rocks samples without added ilmenite in the said pressure range recrystallize from melt without formation of ilmenite. Crystallization of the mixtures produces picroilmenite under all the pressures. In the pressure range of 15-20 kbar titanium- and iron-rich chromaluminium spinel coexists with picroilmenite. In picrite basalt N 349 such spinel crystallizes from melt at a pressure 50 kbar (table 2).

Table 2. **Compositions of coexisting Fe-Ti spinels (wt%) and ilmenites (end members) in the systems rock-ilmenite under high pressures,**

rock	R360	OL-R-52		US-307-731	879	349
pressure	15-20	15-20	37	15-20	15-20	50
spinal						
TiO_2	12.8-17.7	20.8-32.0	35-37	17.6-26.0	23	27
FeO	20.4-28.6	54.8-37.0	20-22	31.5-21.0	61.0-70	41.4-44.1
Al_2O_3	16.0-10.0	13.2-2.0	2-2.5	16.0-8.0	2.4-1.6	12.8-7.8
Cr_2O_3	20.0-26.0	0.6-9.0	7-8г	15.0-26.8	0-0.6	1-0.4
MgO	16.4-15.5	5.0-16.0	27-28.5	14.8-24.0	1.1-1.8	13.8-13
ilmenite						
geikielite	35-46.5	50.0-43.	26	56-65	60-70	30-33.7
hematite	0-0.8	4.5-4.7	6.7	0.6-2.6	1.8-2.2	3.4
Cr_2O_3	3.4-6.2	1.3-1.9	1.3	1-2	1-1.4	0.7-0.2

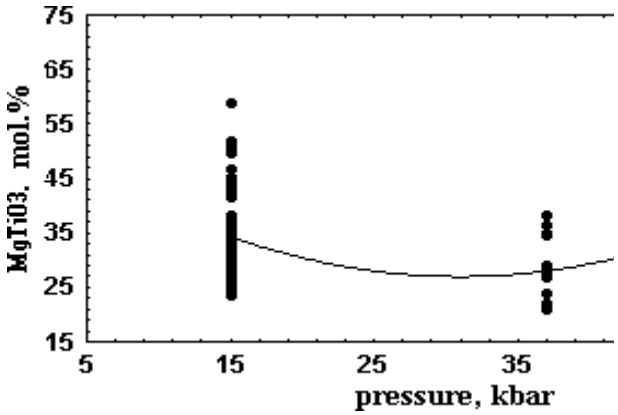

Fig.1a.

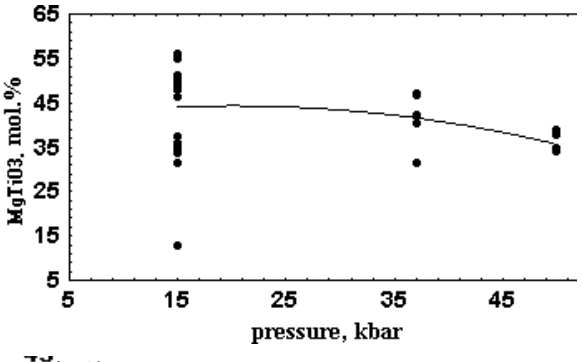

Fig.1b.

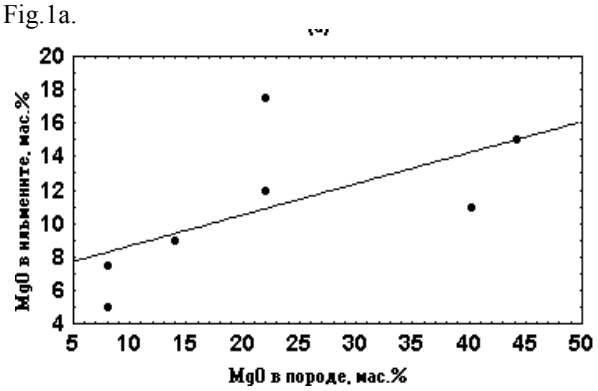

Fig.2a.

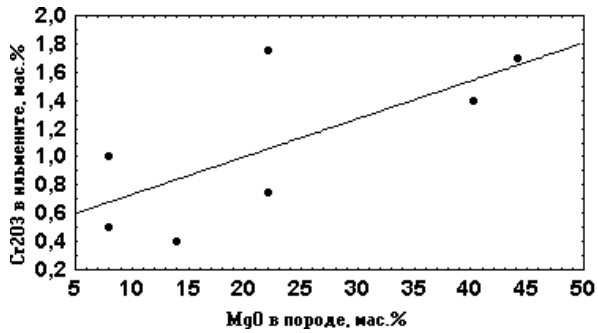

Fig.2b.

Rough estimates show that this paragenesis of ore phases formed at pO_2 below the QFM buffer. As suggested by the published data, in high-pressure solid-state cell (specifically in "clean" runs where the sample was not "contaminated" with an environmental substance) pO_2 is close to the Ni-NiO (NNO) buffer. It should be mentioned that said spinel crystallizes from a carbonate-silicate melt produced by intermixing of the initial mixture melt and incorporated via a graphite heater of a limestone melt. These runs model the situation quite characteristic of thermally active mantle. we shall also mention that titanium-rich chromaluminium spinels similar to those produced in the runs are found among chromites in kimberlites.

The crystallizing picroilmenites contain tiny amounts of ferric iron (hematite in solid solution no more than 4 mol%) as compared with natural minerals of this type. In carbonate-"contaminated" melts there form picroilmenites with a higher concentration of hematite - to 7-7 mol%.

The main result of the experimental studies is the absence of an apparent dependence of magnesiality of picroilmenites on crystallization pressure. The characteristic ratios of the geilielite end member content in solid solution to pressure for ilmenite-picrite basalt and ilmenite-garnet peridotite mixtures are illustrated in fig.1a, b. Also, the correlation has been established between the concentrations of MgO and Cr_2O_3 in ilmenite and MgO in the crystallizing rock (fig.2).

If, factually, more magnesial picroilmenites do form with the depth, this implies the material mantle stratification, i.e. an increase with the depth of a fraction of more magnesial, depleted (or restite) ultrabasic rocks. This conclusion agrees with the ideas of crystallization of such barophilic mineral as diamond in the medium of strongly depleted harzburgites at depths in excess of 150 km.

References:

1. Green D.H., Sobolev N.V. (1975) Contrib. Mineral. Petrol. V. 50. P. 217-229.
2. Bakun-Czubarow N. (1976) Publs. Inst. Geophys. Pol.Acad.Sci. . Ser. A-2, N 101. P. 123-131.
3. Imsland P. (1980) The petrology of the volcanic island Jan Mayen Arctic ocean. Reykjavik: Nordic Volc. Inst., . N 8003. 501 p.
4. Lovering J.F., Widdowson J.L. (1968) Earth Planet. Sci. Lett. . V. 4. P. 310-314.
5. Cawthorn R.G., Groves D.L., Marchant I. Canad. Miner. 1985. V. 23. P. 609-618.
6. Cawthorn R.G., Bristow J.W., Groves D.L. (1989) Min. Mag. . V.53, N 2. P. 245-252.
7. Genshaft Yu.S. (1977) Experimental studies in the field of deap mineralogy and petrology. // M., Nauka, 208p.

[#]Koptev-Dvornikov E.V., Gorbachev P.N. Equation of sulfur solubility in basite melts saturated in sulfide-bearing fluid

[#] The work was sponsored by the RFBR (Project N 99-05-65118)

key words [*low-sulfide solubility immiscibility*]

1. One of the most important sources of platinum metals is low-sulfide noble-metal mineralization in layered intrusions. But, this mineralization is herewith a most difficult-to-detect natural resource. In order to study the formation conditions of this type ores and to predict their occurrence in terms of the COMAGAT one has to derive an equation describing sulfide-silicate liquation. An earlier attempt of deriving an equation for a sulfide-silicate geothermometer showed that the data obtained at temperatures other than 1200°C are fatally lacking (two points only). We therefore performed 25 runs in the temperature range of 1115-1260°C, i.e. the amount of the experimental data of that type was increased by more than one order.

It also appeared that the greatest contribution to the uncertainty was made by an analytic error in sulfur, we therefore concluded that before deriving a geothermometer, we should have to attempt to correct somehow this error.

2. We selected for subsequent treatment the runs on an equilibrium of sulfide and silicate melts for basite compositions at a pressure of 1 atm, including 93 runs at 1200°C (Haughton D.R., Roeder P.L., Skinner B.J. [2]), 8 runs at 1200°C (Buchanan D.L., and Nolan J. [3]), 1 run at 1400°C (Buchanan D.L., Nolan J., Wilkinson N. [4]), and our 25 new runs performed in the temperature range of 1115-1260°C, among them 17 runs were carried out at a pressure 1 kbar, i.e. 128 runs in all.

The pressure runs were included in order to precheck the suggestion of Carmichael [6] that pressure is of no effect on sulfur solubility (should the effect be strong, these points would "bounce" off the 1 atm points).

In order to level uncertainties with respect to sulfur, we first performed a cluster analysis of 102 experimental points at 1200°C. 63 compositions were obtained, 21 of those were clusters each of which consisting of 2-4 samples. The clusters represented combinations of homogeneous samples with low values of intragroup sum of squared distances between the points. The remaining 42 compositions were represented by individual points.

We then analyzed the dependence of sulfur solubility on the run parameters (composition, temperature, oxygen fugacity) so that, based on that dependence, we could "refine" the concentration of sulfur in the runs and use those "refined" values in further calculations of geothermometer.

Earlier an analysis of sulfur solubility was a matter of concern of Naldrett and Li, Wales and Carmichael, Poulson, and Ohmoto. In our work we based on the approach of Ohmoto rather than that of Carmichael and Naldrett because the parameters of the equations proposed by them were sulfur fugacity and iron activity in a silicate melt.

Under the conditions of a sulfide-silicate equilibrium the fugacity of sulfur ceases to be an independent parameter, and calculations of iron activity are cumbersome and, in the absence of a developed model of thermodynamics of silicate melts, not quite reliable.

Ohmoto [7] distinguished two compositional regions for silicate melts (FeO>9 wt% and FeO<9 wt%) where, in his opinion, chemical sulfur solubility reactions are described by different equations. Based on the fact that in the compositional region FeO>9 wt% the dependence $\log X_s = -0.92 + 1.92 \log X_{FeO}$ holds, Ohmoto assumed that two mole-

cules participate in the sulfur dissolution reaction (reasoning from the coefficient at $\log X_{FeO}$). He proposed the following sulfur solubility reaction for that compositional region:

$FeS(sulf.melt) + 2FeO(sil.melt) = Fe_3SO_2(sil.melt)$ (1)

By Ohmoto's suggestion, in this compositional region sulfur occurs as a Fe_3SO_2 complex in a silicate melt.

For the compositional region FeO<9 wt%, where there is no dependence on $\log X_{FeO}$, Ohmoto proposed the reaction

$FeS(sulf.melt) = FeS(sil.melt)$ (2)

For comparison with the results of Poulson and Ohmoto [7] we calculated the logarithms to the base 10 of molar fractions of sulfur and FeO for the 1200°C runs from our sampling. It turned out that the spread of our points was much broader compared to that of Ohmoto (despite some data folding by the cluster method). Possibly, Ohmoto "cleaned" appreciably the initial sampling in order to illustrate his idea. For $\log X_{FeO}$ our coefficient was not an approximate of 2. The approximating straight line has the following form in the compositional region FeO>9 wt%:

$\log Xs = -1.07 + 1.31 \log X_{FeO}$ (3)

This was the first alerting circumstance for us. We attempted to find the dependence of sulfur solubility on temperature, oxygen fugacity, and logarithms of molar fractions of the melt components.

$\log X_s = A/T + B + C \log f_{O2} + \Sigma D_i \ln X_i$ (4)

in order to determine for which of those the coefficient would be close to integral (i.e., stoichiometric) value, in other words, to understand what components participate in the sulfur dissolution reaction under the conditions saturated in a sulfide fluid. Only SiO_2 and Al_2O_3 demonstrated close-to-integral values of the coefficients (approx.2 and 0.5).

3. It became clear for us that Ohmoto's reaction is unlikely to take place. Inasmuch as the participation of sulfur in the reaction of its dissolution is undoubtful, we retained in the logarithmic form only the molar fraction of sulfur in a silicate melt, i.e. we considered the reaction:

$FeS(sulf.melt) = Fe(sil.\ melt)$ (6)

The effect of the remaining components was allowed for in the form of their molar fractions. The effect of the melt polymerization degree was also analyzed.

$\log X_s = A/T + B + C \log f_{O2} + \Sigma F[O/(Si+Al)]$ (6)

In the compositional region with FeO>9 wt% the equation for the dependence of sulfur solubility on the composition and temperature has the form:

$\ln Xs = -1.16 \cdot 10^4/T - 80.0B + 81.4X_{SiO2} + 88.9X_{TiO2} + 79.3\,X_{Al2O3} + 93.7X_{FeO} + 78.0X_{MgO}$ (7)

In the compositional region with FeO<9 wt% the equation for the dependence of sulfur solubility on the composition and temperature has the form:

$\ln Xs = 4.26 \cdot 10^4/T - 32.3B + 0.3 \log f_{O2}$ (8)

Being identical in the form, these equations are fairly different in the set of the terms entering into them. In the iron-rich compositional region an important part is played, along with the temperature, by the concentrations of practically all the silicate melt components, while in the iron-depleted region the solubility of sulfur depends only on the temperature and f_{O2}. The concentrations of sulfur, calculated from eqs (7) and (8) differ from the experimental ones by no more than first hundredths of wt%, i.e. the difference is within analytic uncertainty. The 1 kbar runs did not reveal any systematic deviations from the runs performed at 1 atm.

4. In conclusion, the following can be recommended for further experimental study of saturated sulfur solubility in silicate melts.

1. Experimental study of sulfide-silicate liquation in the temperature range of 1100-1300°C ought to be continued, particularly for the systems with FeO<9 wt%.
2. Experiments are needed in the pressure range of 1-10 kbar under dry and hydrous conditions.
3. Prospectively, it is necessary to experimentally study an equilibrium between a silicate melt and a more compositionally complicated than FeS sulfide fluid (chalcopyrite and pentlandite components should be included).
4. Insufficient accuracy of microprobe determinations of sulfur should be compensated by a large number of measurements for each glass.

References:

1. Koptev-Dvornikov E.V., Vislova T,Ju., Ariskin A.A. (1995) Parameters of sulfide-silicate geothermometer. // Abstr. to the XIII Rus. Meeting on exp. mineral, Chenogolovka, p.149.
2. Haughton D.R., Roeder P.L., Skinner B.J. (1974) Solubility of sulfur in mafic magmas./ Econ.GeoL, V.69, pp. 451-467.
3. Buchanan D.L. and Nolan J. (1979) Solubility of sulfur and sulfide immiscibility in synthetic tholeiitic melts and their relevance to bushveld-complex rocks. / Canad.Miner., V.l7,pp.483-494.
4. Buchanan D.L., Nolan J., Wilkinson N., De Villiers J.P.R. (1983) An experimental investigation of sulfur solubility as a function of temperature in synthetic silicate _melts./ Spec.Publ.Geol.Soc.S.Afr., 7, pp.383-391.
5. Shima H. and Naldrett A.J. (1975) Solubility of sulfure in an ultramafic melt and the relevance of the system Fe-S-O. / Econ.GeoL, 70, pp.960-967.
6. Wallance P. and Carmichael S.E. (1992) Sulfur in basaltic magmas./ Gech. and Cosmoch. Acta, 56, pp.1863-1874.
7. Poulson S.R. and Ohmoto H. (1990) An evaluation of the solubility of sulfide sulfur in silicate melts from experimental data and natural samples./ Chem. Geol., 85, pp.57-75.

[#]Lukanin O.A. Degassing of Cl- and H_2O-bearing acid magmas at their ascent to the surface and crystallization.

key words [*chlorine degassing magmatic fluid rhyolite magma*]

A numerical modeling has been performed for the Cl behaviour in the process of degassing of hydrous rhyolite magmas at decompression- and crystallization - assisted degassing of melts both in closed conditions, when the fluid phase stays in the system, and in open conditions, when the segregating fluid phase escapees from the system. The computer degassing model has been based on generalization of the available experimental data (Kilinc ,Burnham , 1972; Webster, Holloway, 1988; Shinohara et al, 1989; Webster , 1992, 1997; Metrich, Rutherford, 1992; Kravchuk, Keppler, 1994; Malinin, Kravchuk, 1995). The model allows for two important features of fluid-magmatic systems containing Cl and H_2O. First, a strong dependence of partition coefficient of chlorine D_{Cl} (fluid/melt) on both PT conditions and concentration of Cl in a silicate melt. Second the existence of a broad PTX region (P<1.5-2 kbar, T=800-1150^{o}C) of the fluid heterogeneity where it dissociates into two phases coexisting with an alumosilicate melt-substantially aqueous chlorine-containing solution (aqCl) and chloride brine (lqCl). The data calculated with the use of this model demonstrate a number of important features of the Cl behaviour at degassing of acid magmas which are undetectable in the calculations not allowing for the concentration and pressure dependence of D_{Cl} in the process of the magmas ascent and crystallization.

Decompression-assisted degassing. The calculations performed for various concentrations of water and Cl in a melt show that the most important factors for the Cl behaviour are the pressure at which the melt saturation is reached and the degree of the system openness dictating the possibility for the fluid phase to abandon the magma during its ascent. Under the open conditions when all the segregated fluid phase is escaping from the magma with progressing decompression the concentration of Cl in the melt decreases the more considerable the higher are the concentrations of Cl and H_2O (i.e. the higher is P of the melt saturation with the fluid) (fig.1a). In this case the strongest alteration in the Cl concentration in the melt and the fluid phase occurs at first degassing stages. For melts with a low initial concentration of chlorine (<0.1 wt%) and for melts with a relatively low concentrations of H_2O, whose degassing begins at pressures below 1 kbar, the concentration of Cl in the melt in the process of decompression alters insignificantly both under open and closed conditions.

The behaviour of chlorine under the closed conditions when the fluid phase is totally retained in the magma during its ascent has specific features. As shown by the numerical modeling results, under particular initial conditions in the course of the decompression-assisted degassing in the closed system the Cl concentration in the melt goes through a minimum: in the course of decompression the concentration of Cl in the melt first decreases, reaches a minimum and then begins to grow (fig 1b). At further decompression below 0.4-0.5 kbar the Cl concentration in the melt is likely to get stabilized and alters insignificantly. (The model calculations at pressures below 0.3-0.4 kbar are based on yet insufficiently confirmed by experimental data extrapolation of the pressure dependence of D_{Cl}, established at P=0.5-8 kbar, to the low-pressure region).

Crystallization-assisted degassing. The modeling of the crystallization-assisted degassing was performed for isobaric conditions with a preset step of increasing the initial melt crystallization degree. Here we considered a simplified case of "eutectic" crystallisation when the temperature (800^{o}C) and the composition of the residual melt remained constant with respect to petrogenic elements. The calculations show that crystallization of rhyolite melts with high initial concentration of water at high pressures (P>2 kbar) is accompanied by a decrease in the Cl concentration in the melt. An especially dramatic decrease in the Cl concentration occurs in the open conditions where the melt has rather high initial Cl concentrations (fig.2a). If the crystallization-assisted degassing of fluid-saturated melts occurs at pressures below 1.5-2 kbar, then in closed and open systems alike the Cl concentration can grow despite the fact that the D_{Cl} value is always greater in the course of degassing. An increase of the Cl concentration in the melt and the fluid phase in the process of crystallization of the fluid-saturated melts at P<1 kbar can give rise at a particular degassing stage to a chloride-rich phase, i.e. to a heterogeneous fluid (aqCl+lgCl) (fig.2b). One should mention the seemingly paradoxical conclusion that according to the model calculations the degree of the Cl accumulation in the residual melt at the same crystallization degree (P<1-1.5 kbar) is higher in the open system than in the closed one. So, the appearance of the lgCl phase under the open conditions takes place at earlier crystallization stages than under the closed ones. The performed calculations indicate that crystallization of acid magmas in near-surface magmatic chambers (P<1 kbar, H_2O in the melt <3-4 wt%) creates most favourable conditions for the Cl concentration in residual melts and fluids segregating from the magma.

References:

1. Kilinc I.A., Burnham C.W. (1972) //Economic Geology 67, 231-235
2. Malinin S.D., Kravchuk I.F. (1995).// Geokhimiya, No.8, p. 1110-1130.
3. Metrich N, Rutherford M.J. (1992) //Geochim. Cosmochim. Acta, V.56, pp. 607-616.
4. Shinohara H., Ilyama J.T, Matsuo S. (1989) // Geochim. Cosmochim. Acta, V.53, pp. 2617-2630.
5. Webster J.D. (1992) Geochim. Cosmochim. Acta, V.56, pp. 659-678.
6. Webster J.D. (1997) J. Petrol., V.38, N.2, pp.l793-1807.

[#] The work has been sponsored by the RFBR (Grant N 96-05-65467)

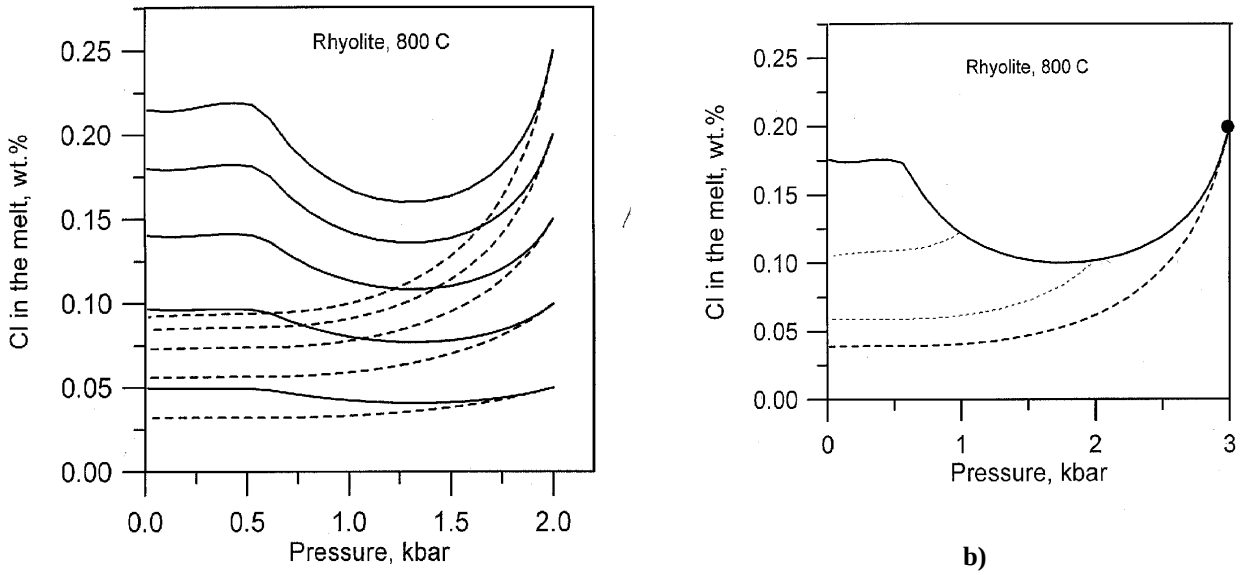

a) b)

Fig.1.a,b. Trajectories of the Cl concentration alteration in a rhyolite melt at decompression-assisted degassing. a- Decompression-assisted degassing of the rhyolite melt of different initial concentrations of Cl reaching the fluid-phase saturation at 2 kbar (initial concentration of H_2O in the melt is ≈5.5 wt%). The solid line stands for closed conditions, the broken line stands for open conditions. b- Decompression-assisted degassing of the rhyolite melt reaching the fluid-phase saturation at 3 kbar (initial concentrations of Cl equal 0.2 wt%, H_2O=7 wt%). The solid line stands for closed conditions, the broken lines are degassing under open conditions. Thin broken lines show the cases where the magma ascent to the surface occurs under open conditions beginning with a certain pressure (2 and 1 kbar). The figure demonstrates the effect of the openness degree on the Cl concentration in the melt near the surface.

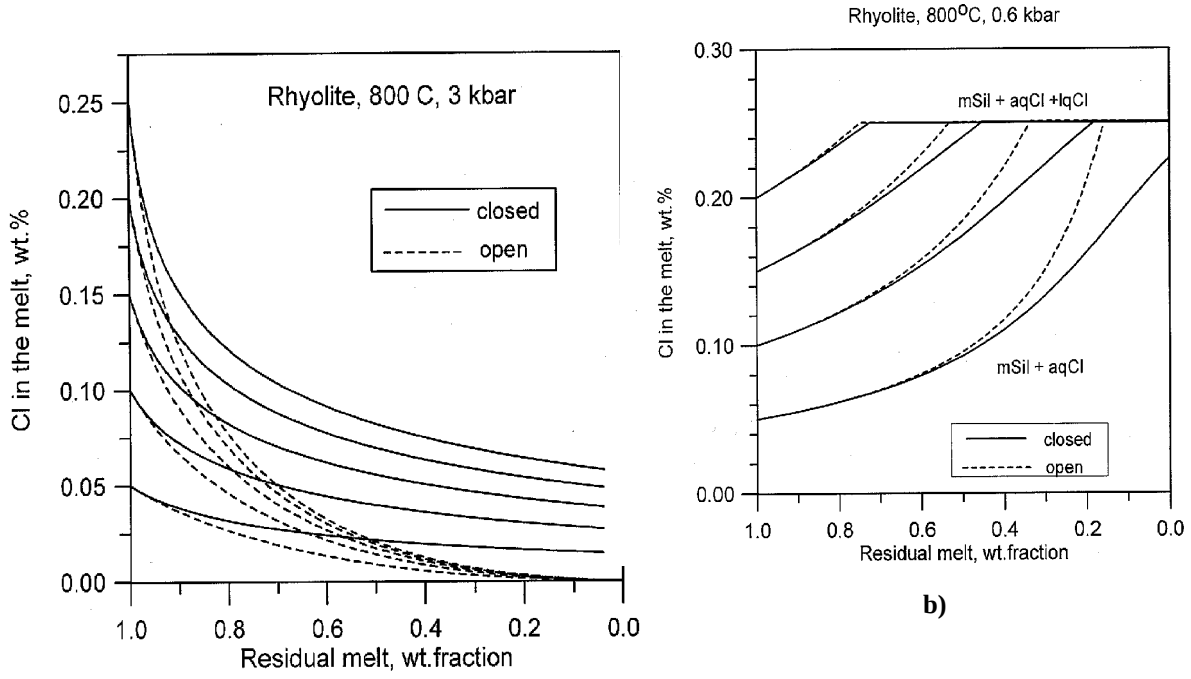

a) b)

Fig.2 a,b. Trajectories of the Cl concentration alteration in a residual rhyolite melt in the process of the crystallization-assisted degassing. a -crystallization-assisted degassing of fluid saturated rhyolite melts with different initial concentrations of Cl at 3 kbar (initial concentration of H_2O in the melt ≈ 7wt%). The solid line is closed conditions, the broken line is open conditions. b- crystallization-assisted degassing of fluid- saturated rhyolite melts with different initial concentration of Cl at 0.6 kbar (initial concentration of H_2O in the melt ≈ 2.5wt%). The solid lines are closed conditions, the broken lines are open conditions. In rhyolite melts with the initial Cl concentrations >0.5 wt% in the process of crystallization the concentration of Cl in the residual melt grows reaching

0.25 wt%. The fluid phase gets heterogenized herewith and at further crystallization the aqueous chlorine-containing solution (aqCl). and chloride brine (lgCl) are in equilibrium with the silicate melt (mSil).

Semyonov I.V. Modelling of the partial melting level in the upper mantle during apperance of basalts of urals ophiolites and MOR tholeiites (on the data of REE content in complentary triad lherzolite = basalt + harzburgite).

key words [mid-oceanic ridge ophiolite upper mantle partial melting tholeiite lherzolite harzburgite]

The question of determining the level of partial melting in the mantle during the appearance of tholeiite basalts under modern mid-oceanic ridge (MOR) and also in paleoanalogues of these formations – ophiolite associations of modern continents – remains disputable. Our researches showed that not the partial melting in the upper mantle on the whole, but partial melting of different-depth mineral associations of upper mantle – plagioclase lherzolites, spinel lherzolites and garnet peridotites should be the matter of discussion. Just as the result of partial melting of each of them the fusions different on chemical composition with characteristic correlations of REE contents [4] formed.

The authors attempted modelling the level of partial melting in the upper mantle proceding from the conception of complementarity of the triad lherzolite = basalt + harzburgite with reference to the processes under the MOR and ophiolites based on the established in these rocks REE contents. While calculating "the percent" of partial melting as the initial values for lherzolites and harzburgites REE concentrations in lherzolites and harzburgites lost by the mantle in the MOR spreading zones have been used [1].. The carried out comparison shows [4] that REE contents in lherzolites and harzburgites of ophiolite massif in particular Troodos (Cyprus), Othris and Pindos (Greece), Sikoku islands (Japan), the Urals (Russia) and other ones are compareable with those in MOR. Lherzolites and harzburgites of MOR and ophiolites are inhomogeneous in REE content. Two varieties of each of these rocks were established , differing in REE content. For lherzolites of the first variety the REE content close to chondrite one (primary lherzolite – undepleted mantle) is characteristic. The second one features a sharp deficit of light REE in chondrite and characteristic anomalies to separate elements (exhausted lherzolite – weakly depleted mantle). In harzburgites as restites one variety is sharply enriched (relatively chondrite) with heavier REE, the second one is characterized by W-like REE distribution with positive Eu-anomaly.

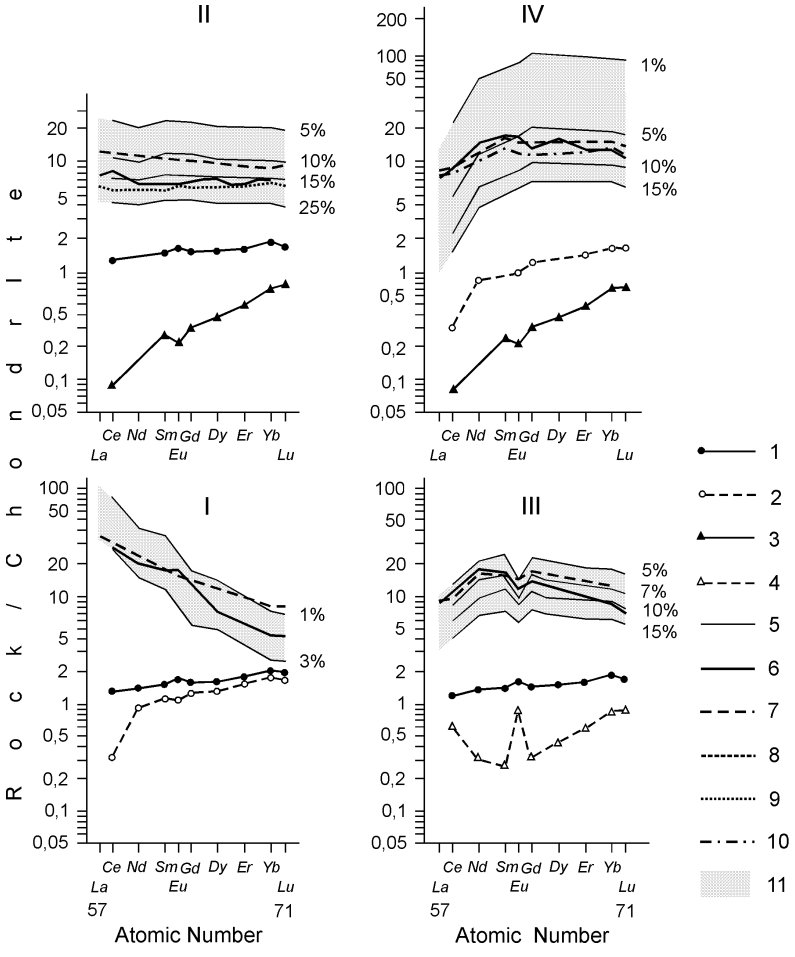

Fig. 1. Comparison of REE fractionation diagrams , normalized to chondrite in tholeiite basalts of the Urals ophiolite association and MORB (I, II, III and IV types) with fractionation diagrams plotted on calculating the REE contents in basalts.

1 – REE content in primary lherzolites ; *2* – the same in exhausted lherzolites; *3*- the content of harzburgites, enriched with heavy rare-earth elements; *4* – the same, with W-like REE distribution; *5* – calculated REE contents in basalts, corresponding to different "percents" of melting with the given REE content in initial lherzolite and restite; *6* – average REE contents in basalts of the Urals ophiolite association fdr each of the four types of distribution; *7* – average REE contents in tholeiites of Mid-Atlantic Ridge: I type – at the latitude of 38-40^0 N (middle from samples F, B, C on [10]); II type - at the latitude of 35-36^0 N (sample G on [10]); III type – at latitudes of 22^0 N, 23^0 N, 6^0 N, 6^0 S, 21^0 S (average of samples 2-5 and 3-2 [7]); sample from the well 395 and 395A DSDP of a trip 45 on [9]; sample from the wells 396 and 396B of a trip 46 on [6]; sample D-4, D-3 and D-2-1 on [7]; with IV type – at the latitudes of 30-35^0 N (average of samples M, N, O on [10]; *8-10* – averagee REE contents in DSDP tholeiites of a trip 37 [5]: *8* – in basalts of the wells 332A, 332B, 333A, 334; *9* – in basalts of the well 332B; *10* – in basalts of the well 335.

Tholeiite basalts of the Urals ophiolite association and the MOR tholeiites have been considered as the products of partial melting in the mantle. The researches showed that the REE content both in ophiolite basalts and in MOR substantially varies. However, these variations are not chaotic ones, but described in both cases by four identical types of REE distribution. The I type is characterized relative chondrite by weak increase in more and more light REE; the II type - by practical absence of differentiation ; the III type – by the enrichment in Nd and Sm with La and Ce deficit; the IV type – by practical absence of fractionation from Nd to Sm upon La and Ce deficit. While determining "the percent" of melting in the mantle under the MOR the tholeiites from Mid-Atlantic and Mid-Indian ridges (with I, II, III and IV types of REE distribution, from the wells 37, 45 and 46 of "Glomer Chellendger" trip (with II and IV types of distribution) were used as the examples. Since the Urals ophiolite basalts and MOR tholeiites are characterized by the same types of REE distribution, then it seemed reasonable to calculate the "percent" melting in the mantle during the appearance of basalt melts with each of the four types of distribution.

During calculations the primary lherzolite of the IV type – exhausted lherzolite has been taken as the initial lherzolite for the basalts of I, II and III types. As a restite for basalts of I type exhausted lherzolite was used, of II and IV types – harzburgit with higher compositions of heavy elements, of III type – harzburgite with W-like REE distribution. The essence of the accepted approach to determination of partial melting in the mantle is as follows. REE composition in basalt fusions will be considered as the difference between REE contents in initial lherzolites and restites. For calculating the possible REE concentrations in basalt fusion , corresponding to n-% level of partial melting the obtained difference of concentrations should be divided into the value of melting "percent" (n-%) and multiplied by 100. Then we take normalization of the calculated concentrations to chondrite and plot the corresponding diagrams. Then compare the diagrams of the calculated concentration with the diagrams of real concentrations. The value used for plotting the calculation diagram, in the best way approximating one of four real types of REE distribution in basalts has been taken as the most probable average"percent" of melting.

According to the calculations made (Fig. 1) the Urals ophiolite association basalts and MOR tholeiites with the I type of REE distribution can occur at 1-3%, with II type – at 10-15%, with III type – at 7-10% melting of the primary lherzolite , with IV type – at 5-10% melting of the exhausted lherzolite. The obtained values of the "percent" of melting are in accordance with the value of the average "percent" of melting under the MOR, obtained from petrochemical [2] and geochemical [8] data. They are also compareable with the results of calculations made using seismic researches and data of electrogeomagnetic probing. According to these calculations, in upper layers of astenosphere up to the depths of about 30 km under modern mid-oceanic ridges the share of liquid phase makes up 10-15% and decreases up to 1-3% at the depths of 60-80 km [3].

References:

1. Balashov Ju.A. (1975) Geochemistry of rare-earth element. // Moscow: Nauka, , 276 pp.
2. Dmitriev L.V. (1980) Variations of content of the oceans mantle // Magmatic and metamorphic rocks of the Ocean bottom and their genesis. Moscow, p.20.
3. gLukashevich I.P., Gorshkov A.G.. (1989) Peculiarities of tholeiite magmatism in connection with evolution of mid-oceanic ridges // Geotectonics, N 6, pp. 105-111.
4. Semyonov I.V. (1990) REE content in Urals paleooceanic basalts and oceanic tholeiites as the indicator of depths of partial melting in the upper mantle. // Sverdlovsk, 66 pp.
5. Aumento F., Melson V.G., Hell J.M., Baugault H., Dmitriev L., Fischer J.F., Flower M., Howe R.C., Hyndman R.D., Miles G.A., Robinson P.T., Wright T.L. (1977) Site 332, [pp. 15-200]. Site 333 [pp. 201-239]. Site 334 [pp. 239-288]. Site 335 [pp. 289-326] //Init. Rep. of DSDP, v. 37, pp. 15-326.
6. Dungan M.A., Rhodes J.M., Long P.E., Blanchard D.P., Brannon J.C., Rodgers K.V. (1979) The petrology and geochemisrtry of basalts from site 396, lege 45 and 46 of the Deep Drilling Project //Init. Rep. of DSDP, v. 46, pp. 89-113.
7. Frey F.A., Haskin M.A., Poetz J.A., Haskin L.A. (1968) Rare-earth abundances in some basic rocks //J. Geophys. Res., v. 73, N 18, pp. 6085-6093.
8. Parkinson I. J., Pearce J.A. (1998) Peridotites from the Izu-Bonin-Mariana Forearc (ODP Leg 125): Evidence for Mantle Melting and Melt-Mantle Interaction in a Supra-Subduction Zone Setting //Journal of Petrology, v. 39, N 9, , pp. 1577-1618.
9. Rhodes J.M., Blanchard D.P., Dungan M.A., Rodgers K.V., Brannon J.C. Chemistry of leg 45 basalts //Init. Rep. DSDP, 1979, v. 45, pp .447-459.
10. Schilling J.G. (1975) Azores mantle blob: rare earth evidence //Earth. Planet. Sci. Lett., v. 25, N 2, pp. 103-115.